INHIBITORY EFFECT OF SOME ADDITIVES ON METHANE-AIR FLAME

By

Ismail Ibrahim Hasan Hdaib

Supervisor

Dr. Mohammad Ahmad Hamdan, Prof.

Co-Supervisor

Dr. Jehad Ahmad Yamin

This Dissertation was Submitted in Partial Fulfillment of the Requirements for the Doctor of Philosophy Degree in Mechanical Engineering

Faculty of Graduate Studies

The University of Jordan

June, 2009

COMMITTEE DECISION

This Dissertation (Inhibitory Effect of Some Additives on Methane-Air Flame) was Successfully Defended and Approved on 10 / 5 / 2009.

Examination Committee	Signature
Dr. Mohammad Ahmad Hamdan, (Supervisor) Prof. of Mechanical Engineering	----------
Dr. Jehad Ahmad Yamin, (Co-Supervisor) Assist. Prof. Mechanical Engineering	----------
Dr. Ali Badran, (Member) Prof. of Mechanical Engineering	----------
Dr. Adnan Jaradat, (Member) Assoc. Prof. of Mechanical Engineering	----------
Dr. Ahmad Al-Salaymeh, (Member) Assoc. Prof. of Mechanical Engineering	----------
Dr. Ahmad Abu-Jrai, (Member) Assist. Prof. of Mechanical Engineering (Al-Hussein Bin Talal University)	----------

تعتمد كلية الدراسات العليا
هذه النسخة من الرسالة
التوقيع.....التاريخ.....

To

My Mother, my father,

Beloved small family

Shahd, Reem, Ibrahim, Ziad,

brothers and sisters,

with love and gratitude

AKNOWLEDGEMENT

Initially, I like to completely admit the full support of Prof. Mohammad A. Hamdan, the man who gives a lot of patient, help, encouragement, guidance, and father role in this work. He started with me before the research and continued until last moments.

Secondly, I would like to express my full gratitude to Dr. Jehad A. Yamin, the person who provides a brotherhood relation when co-advising this research; he was one of the most helpful people I ever know, in his opinions, ideas, solutions, and suggestions.

Fortunately, I found Dr. Ahmad A. Sakhrieh. He made it easy to deal with software, and to translate knowledge to this work. I appreciate the support received from Dr. Musa O. Abdullah, for his help in instrumentation search and how to fix things for our work requirement. Many thanks to you Dr Musa. Also, A special thanks goes to the group of B.Sc. students who helped in doing the experiments.

This work could not be done without the support of my big family. You were the most helping people whom I can find in my life. Your thoughtfulness increases the faith I need to face the days to come with courage and hope. Also you were the sweets taste of my pleasure and happiness. For all what you did for me, I do thank you very much.

During a time like this I realize how much my children mean to me. Your kind expression of sympathy will always be remembered. Life's path is more easily traveled in the company of children like you. Thank you for your kindness.

TABLE OF CONTENTS

Subject	Page
Committee Decision	ii
Dedication	iii
Acknowledgement	iv
Table of Contents	v
List of Tables	vi
List of Figures	vii
List of Abbreviations or Symbols	ix
List of Appendices	xi
Abstract	xii
Introduction	1
Radicals and Combustion Reactions	2
Chapter One Literature Review	5
Chapter Two Combustion and Flames	12
2.1 Review of Combustion and Flames	12
2.2 Stoichiometric Reaction	12
2.3 Flame Temperature	13
2.4 Laminar Flame Speed	16
2.5 Flames Classifications	20
2.6 Structure of Premixed Flame	21
2.7 Flammability Limits	23
2.8 Inhibitors and Retardants	25
2.9 Theoretical Model and Algorithm	27
2.9.1 Governing Equations	28
2.9.2 Boundary Conditions	29
2.9.3 Algorithm Structure and Modification	30
Chapter Three Experimentation and Data Observations	33
3.1 Experimental Setup	33
3.1.1 Flame Speed Measurements	35
3.1.2 Some Methods for Flame Speed Measurements	37
3.2 Experimental Procedure	39
3.3 Experimental Observations	40
3.4 Experimental Results	44
Chapter Four Discussion of Results	51
4.1 Model Validation Through Experimental and Theoretical Data	51
4.2 Distance, Velocity and Percentage of Inhibition Simulation	55
4.2.1 Addition of CO_2	55
4.2.2 Addition of N_2	57
4.3 Comparison of some additives	59
4.4 Chemical Kinetics Comparison	63
4.5 Uncertainty Analysis	69
Conclusion and Summary	72
References	74
Appendices	79
Abstract (in Arabic)	84

LIST OF TABLES

NUMBER	TABLE CAPTION	Page
2.1	Lower and upper flammability limits of some fuel gases indicated for gas and air at 20°C and atmospheric pressure.	24
3.1	Laminar flame speeds for various pure fuels burning in air at stoichiometric composition and standard temperature and pressure.	37
3.2	Methane-air flame speeds as CO_2 inhibitor is used.	49
3.3	Methane-air flame speeds as N_2 inhibitor is used.	49
4.1	Comparison between moles consumption for radicals at Φ=0.65 and 20% inhibition percentage.	68
4.2	Uncertainty analysis for all experimental F/A ratios.	71

LIST OF FIGURES

NUMBER	FIGURE CAPTION	Page
2.1	Distribution of the methane adiabatic flame temperature against A/F at ambient pressure and temperature	15
2.2	Distribution of methane adiabatic flame temperature against initial air temperature at ambient pressure and stoichiometric air-fuel ratio	15
2.3	Distribution of methane adiabatic flame temperature against pressure at ambient temperature and stoichiometric conditions	16
2.4	Distribution of methane flame speed against pressure at ambient temperature and stoichiometric A/F ratio	18
2.5	Distribution of methane flame speed against inlet air temperature at ambient pressure and stoichiometric A/F ratio	19
2.6	Distribution of methane flame speed against A/F ratio at ambient pressure and temperature	19
2.7	Calculated inner structure of a laminar, stoichiometric, methane-air flame	22
2.8	Normalized burning velocity of premixed $CH_4/O_2/N_2$ flames inhibited by CO_2, CF_3Br, $Sn(CH_3)_4$, $SnCl_4$, MMT, TMP, and $Fe(CO)_5$. (T_i = 353 K for all data except $Sn(CH_3)_4$ and $SnCl_4$ which are at 298 K). Lines are curve fits to data	26
2.9	Algorithm of modified software with developed data files and processors	31
2.10	Copy of GRI-Mech used in modeling and simulation.	32
3.1	Picture of experimental setup used	33
3.2	Picture of some pressure gauges used in the apparatus	34
3.3	Picture of vacuum pump used in experimental setup	34
3.4	Picture for photovoltaic cell and connection to a wooden stand	35
3.5	Illustrated drawing for flammability limits with burning velocity	36
3.6	Photo of the software flame speed interface	38
3.7	Photo a flame when ignition was started (frame 1), after 0.1333 second (frame 5) and after 0.3535 second of first frame (frame 9)	39
3.8	Photo of methane-air flame at ignition point	41
3.9	Photo of methane-air flame color without addition of inhibitors	41
3.10	Photo of methane-air flame color with addition of CO_2	42
3.11	Photo of frames for nitrogen inhibited methane air flame	43
3.12	Methane-air rich and lean flammability limits as CO_2 inhibitor used	45
3.13	Methane-air rich and lean flammability limits as N_2 inhibitor used	45
3.14	Flame speed at methane-air ratio = 8%, 10.5% and 14% while using different CO_2 quantities	47

3.15	Flame speed at methane-air ratio = 8%, 10.5% and 14% while using different N_2 quantities	48
4.1	CH_4–air flame model verification at different % of CO_2 (velocity vs F/A ratio) curve	52
4.2	CH_4–air flame model verification at different % of N_2 (velocity vs F/A ratio) curve	52
4.3	Flame speed at methane-air ratio (8%) using different quantities of CO_2, N_2, and SO_2	53
4.4	Flame speed at methane-air ratio (10.5%) using different quantities of CO_2, N_2, and SO_2	54
4.5	Flame speed at methane-air ratio (14%) using different quantities of CO_2, N_2, and SO_2	54
4.6	Simulated Inhibition of lean CH_4–air flame with CO_2 inhibitor	55
4.7	Simulated Inhibition of rich CH_4–air flame with CO_2 inhibitor	56
4.8	Simulated Inhibition of lean CH_4–air flame with N_2 inhibitor	57
4.9	Simulated Inhibition of rich CH_4–air flame with N_2 inhibitor	58
4.10	Simulated Inhibition of rich CH_4–air flame with SO_2 inhibitor	59
4.11	Simulated Inhibition of lean CH_4–air flame with SO_2 inhibitor	60
4.12	Simulated Inhibition of rich and lean CH_4–air flame with CO_2 inhibitor	61
4.13	Simulated Inhibition of rich and lean CH_4–air flame with N_2 inhibitor	62
4.14	Simulated Inhibition of rich and lean CH_4–air flame with SO_2 inhibitor	62
4.15	Simulated 20% (CO_2, SO_2, and N_2) additive H-radical to methane-air flame at $\Phi = 0.65$	63
4.16	Simulated 20% (CO_2, SO_2, and N_2) additive O-radical to methane-air flame at $\Phi = 0.65$	64
4.17	Simulated 20% (CO_2, SO_2, and N_2) additive OH-radical to methane-air flame at $\Phi=0.65$	65
4.18	Simulated 20% (CO_2, SO_2, and N_2) additive CO-radical to methane-air flame at $\Phi=0.65$	65
4.19	Simulated 20% (CO_2, SO_2, and N_2) additive CH_3-radical to methane-air flame at $\Phi=0.65$	66
4.20	Simulated 20% (CO_2, SO_2, and N_2) additive CH_2-radical to methane-air flame at $\Phi=0.65$	67
4.21	Simulated 20% (CO_2, SO_2, and N_2) additive CH-radical to methane-air flame at $\Phi=0.65$	67
4.22	Simulated 20% (CO_2, SO_2, and N_2) additive CH_2O-radical to methane-air flame at $\Phi=0.65$	68

LIST OF ABBREVIATIONS OR SYMBOLS

Abbreviation		Units
A	Arrhenius Constant	-
A, B, AB	Chemical species	-
AF	Air to fuel ratio	-
AIT	Auto ignition temperature	K
c	*Constant*	-
E_A	Activation energy	J
FTIR	Fourier transform infrared	-
ID	Inside diameter	m
k	Reaction rate coefficient	-
k_f	Forward reaction rate coefficient	-
LEL	Lower explosive limit	%(v/v)
LFL	Lower flammability limit	%(v/v)
M	Third body (radical)	-
P	Pressure	Pa
PLC	Programmable logic controller	-
PPM	Parts per million	ppm
S, S_L	Flame speed	m/s
STP	Standard temperature and pressure	-
Stoich.	Stoichiometric	-
T	Temperature	K
T_{adiab}	Adiabatic flame temperature	K
T_i	Initial air temperature	K
T_m	Mixture temperature	K

u	**Velocity of unburned gas**	**m/s**
UEL	**Upper explosive limit**	**%(v/v)**
UFL	**Upper flammability limit**	**%(v/v)**
y	**Mole fraction**	**specie moles/total moles**

Greek Symbols

Φ	**Equivalence ratio**	**-**
λ	**The inverse of the air number**	**-**
δ	**Thickness of reaction zone**	**-**

LIST OF APPENDICES

NUMBER	APPENDIX	Page
A.1	Chemical kinetics software	79
A.2	GRI-Mech	79
A.3	Some fuels flammability limits	80
A.4	Thermodynamic data files	80
A.5	Transport data files	81
A.6	CO_2 chemical reactions	81
A.7	N_2 chemical reactions	82
A.8	SO_2 chemical reactions	82
A.9	Low temperature (<1500k) reaction pathway diagram for combustion of CH_4	83

INHIBITORY EFFECT OF SOME ADDITIVES ON METHANE-AIR FLAME

By

Ismail Ibrahim Hasan Hdaib

Supervisor

Dr. Mohammad Ahmad Hamdan, Prof.

Co-Supervisor

Dr. Jehad Ahmad Yamin

ABSTRACT

Experimental and theoretical studies of the inhibitory effects of some local gases on the flame propagation of premixed methane-air mixture in a vertical tube were conducted. The inhibitors used in this study were carbon dioxide, nitrogen, and sulpher dioxide. This was done by finding the flammability limits and flame speed for both pure methane-air as well as methane-air-inhibitor mixtures. The inhibitors' concentration was varied from 5% to 20% by volume.

An experimental setup was built from pyrex glass and measuring devices were located at different positions, they were used to find flame speed and flammability limits. Gas cylinders used were methane of 99.94% purity, carbon dioxide with 99.92% purity, and nitrogen with 99.93% purity. At first, the baseline for comparison was set by studying the combustion of pure methane-air and its flame speed as well as flammability limits were measured. Then, known amounts of inhibitor were added each

one in turn and the same data was measured. All the above experiments were conducted under atmospheric conditions.

It was found that the flame speed for pure methane-air mixture was measured to be about 0.40 m/s. This value decreased when inhibitors were added. The lower flammability limit (LFL) was found to be 5.0% and the upper flammability limit (UFL) was 14.0%. When CO_2 was used in (5, 10, 15, and 20%) the LFL's were (5.4, 5.8, 6.1, and 7.1%) respectively, and the UFL's were (13.2, 12.5, 11.6, and 10.0%) respectively. When using N_2 in same percentages, the LFL's were (5.3, 5.6, 6.0, and 6.7%) respectively, and the UFL's were (13.5, 13.0, 12.8, and 12.0%) respectively.

To have an inner view of what happened inside the reaction zone, a theoretical model consisted of the latest GRI-Mech methane combustion reaction mechanism was used. All the data files e.g. thermodynamic and transport properties, species chemistry input, tube geometry and initial conditions and the reaction mechanism were set and verified against experimental data. These files (including the reaction mechanism) were modified when using each inhibitor in turn (except for SO_2) and verified against the experimental results.

It was found that CO_2 has the higher inhibitory effect and N_2 gas has the lower inhibitory effect among inhibitors used in this work. SO_2 is an appreciated inhibitor compared to nitrogen but is still weak when compared to carbon dioxide. Inhibition rank of the three inhibitors used is $CO_2 > SO_2 > N_2$.

Introduction

In the early 1990's it was estimated that 29 000 injuries and 4 500 deaths were caused by fires each year in the United States alone and that the total global cost is over $100 billion annually. Today fires in structures occur every 60 seconds, residential fires every 82 seconds, every 85 seconds in a vehicle and every 34 seconds in an outside property. 1.8 million fires a year in the United States resulted in $10 billion in property damage, 3,570 civil deaths and 21,875 injuries in 1999, down from the early 1990's [1].

Jordan and due to the continuously escalating imported fuel cost, is seriously utilizing natural gas as a major source of energy, especially as it imported from Egypt. Natural gas consists of methane, ethane, propane, and several hydrocarbon compounds. Methane composes almost 70% of that natural gas. Therefore, the subject of methane fires is becoming a major concern to many. Due to great risk of fire to humans and their possessions, new methods are being continuously investigated and developed to prevent fires and reduce their effects. [1].

It is well known that halogen compounds have excellent inhibitory effect on fire. However, the production of the widely used but ozone-destroying fire-fighting agent Halon 1301 (CF_3Br) has been banned. Environmental concerns related to the destruction of stratospheric ozone has initiated the phasing out of fire-fighting agent Halon 1301 (CF_3Br) from the US army inventory. 2-H heptafluropropane (C_3F_7H, FM-200, HFC227ea) has been identified as one of the alternative agents for unoccupied spaces of critical installations formerly protected by Halon 1301. For occupied spaces, where fires must be suppressed in a short period of time (250ms), to minimize exposure to extreme heat and toxic fumes, a mixture of C_3F_7H with sodium bicarbonate ($NHCO_3$) or water with potassium acetate has been chosen as a leading Halon replacement candidate [2].

There remains a need for alternative fire suppressants in a variety of applications. Some metal compounds have been shown to be up to two orders of magnitude more effective than production of -the widely used but ozone-destroying compound- (CF_3Br) at reducing the burning velocity of premixed flames. It is of interest to understand their mechanisms of inhibition to determine if there are ways that they might be used as additives to fire suppressant blends, for both occupied and unoccupied spaces [1].

Reviewing the literature available, it is noticed that not much research was conducted to study the flame and how it can be utilized for combustion control. Combustion is usually a gas phase phenomenon. Volatile combustible species oxidize exothermically in the gas phase. Afterglow or glowing combustion is a form of non-gas phase combustion. Here the substrate is oxidized in the condensed phase to form both solid and gaseous products. This usually takes place at temperatures well below the ignition temperature of the material. For instance, the carbon residue rich material is oxidized in the solid phase [1].

Radicals and Combustion Reactions

Chemical chain reactions involve the production of a radical species that subsequently reacts to produce another radical. This in turn, reacts to produce yet another radical.

This sequence of events or chain reaction continues until a reaction involving the formation of a s species from two radicals breaks the chain [3].

Radicals play one of the two important roles, either accelerating the reaction rate, or decelerating it. The accelerating species have the name radicals, while the decelerating ones have the name retardants or inhibitors.

Radicals or Free Radicals are reactive molecules, or atoms that have unpaired electrons. Some of the basic features of chain reactions are illustrated by exploring a hypothetical chain mechanism, which is globally represented as [3],

$$A_2 + B_2 \rightarrow 2AB \quad (1)$$

The chain initiation reaction is [3],

$$A_2 + M \xrightarrow{k_1} A + A + M \quad (2)$$

And the chain propagation reaction is [3],

$$A + B_2 \xrightarrow{k_2} AB + B \quad (3)$$

$$B + A_2 \xrightarrow{k_3} AB + A \quad (4)$$

The chain terminating reaction is [3],

$$A + B + M \xrightarrow{k_4} AB + M \quad (5)$$

Where, "***M"*** may be any molecule and is frequently referred to as a third body, "A" and "B" are species while, ***"k"*** is the reaction rate coefficient.

In the early stages of reaction, the concentration of product "AB" is small, as are the concentrations of "A" and "B" throughout the course of the reaction, thus the reverse reaction can be neglected [3].

The effectiveness of the inhibitor was tested using flame speed measurement. The characteristics of flames due to inhibitory effects and how the inhibitor is going to retard the flame of methane-air combustion were studied experimentally and theoretically. The experimental test rig and operation was built in the laboratory for this purpose.

In order to achieve the desired aims, the present study is classified into five chapters. Introductory part (Introduction of the inhibition need, concepts of chain reaction and retardants, effectiveness of inhibition measurement). Literature review

(Chapter One provides a review of studies in that subject, and a scope of similar work presented) Review of combustion and flames (Chapter Two presents a review of combustion and flames with some scientific facts, considering laminar flame propagation). Experimentation and data (Chapter Three considers an experimental setup and its equipment, the procedure, of doing experimentation are described, and observations on inhibitors) Discussion of computer simulation (Chapter Four presents the discussion of results and data. The theoretical and experimental results are compared in this chapter) Conclusion (Finally, conclusions with recommendations for further and future work.

Chapter One

Literature Review

Nogueira and Fisher [4] studied the impact of dimethyl methylphosphonate (DMMP) in a premixed methane/oxygen/N_2-Ar flame in a flat flame burner slightly under atmospheric pressure at two different equivalence ratios: rich and slightly lean. CH_4, CO, CO_2, CH_2O, CH_3OH, C_2H_6, C_2H_4, and C_2H_2 profiles were obtained with a Fourier Transform Infrared (FTIR) spectrometer. Gas samples analyzed in the FTIR were extracted from the reaction zone using a quartz microprobe with chocked flow at its orifice. Flame calculations were performed with two existing detailed chemical kinetic mechanisms for organophosphorus combustion. DMMP addition caused all profiles except that of CH_3OH to move further away from the burner surface, which can be interpreted as a consequence of a reduction in the adiabatic flame speed. Experimentally, the magnitude of the shift was 50% for this near-stoichiometric flame than for the rich flame. Experimental CH_3OH profiles were four to seven times higher in the doped flames than in the undoped ones. The magnitude of its effect was not predicted in the calculations, suggesting a need for further mechanism development. Otherwise, the two mechanisms wee reasonably successful in predicting the effects of DMMP on the flame.

Babushok et al [5] modeled synergistic effects in flame inhibition by 2-H heptafluoropropane blended with sodium bicarbonate. Flame equilibrium calculations demonstrated that for mixture compositions $[C_3F_7H]/[NaHCO_3]$, the main product containing sodium atom at the equilibrium is NaF. The amount of HF acid scavenged by sodium in the flame reaction zone is relatively small due to the small [Na]/[F] ratio. The advantage of the use of blend suppressants is the increase of the suppression

effectiveness while blend provides reasonably good physical properties for its release by fire extinguishers. Thus, decreased HF concentration level during fire suppression by [C_3F_7H]/[$NaHCO_3$] blend is the result of increased inhibition effectiveness of heptafluoropropane blended by sodium bicarbonate with minor contributions of solid particle-gas phase HF scavenging during mixing of cooled combustion products with the surrounding post-suppression atom sphere that contains fire suppressant after flame extinguishment.

Linteris et al [6] studied the inhibition of premixed methane flames by manganese and tin compounds (MMT, TMT) on the burning velocity of methane/air flames. They compared $Fe(CO)_5$ and CF_3Br and demonstrated that manganese and tin containing compounds are effective inhibitors. The inhibition efficiency of MMT was about a factor of two less than that of iron pentacarbonyl, and that of TMT was about 26 times less effective, although TMT was still about twice as effective as CF_3Br. They concluded that there exist conditions for which both MMT and TMT showed a loss of effectiveness beyond that expected because of radical depletion, and the cause was believed to be particle formation. Kinetic models describing the inhibition mechanisms of manganese- and tin containing compounds were suggested. Simulations of MMT- and TMT- inhibited flames showed reasonable agreement with experimental data.

Macdonald et al [7] showed that phosphorus containing compounds (PCCs) are proposed as viable alternatives to current, ozone-destroying inhibiting agents. They used an opposed-jet burner apparatus to study the effectiveness of two low vapor pressure PCCs, dimethyl methylphosphonate (DMMP) and trimethyl phosphate (TMP), in extinguishing a nonpremixed methane-air flame. The global extinction strain rate was determined as a function of dopant loadings. Tests were also, conducted using nitrogen as an inert additive for reference. Results demonstrated that these PCCs were significant

inhibitors of nonpremixed methane-air flames when introduced into the oxidizer stream. 40 times more effective than nitrogen on a molar basis. A novel technique for measuring extinction strain rate while maintaining a constant dopant level in one gas stream was developed.

Babushok et al [8] presented a paper that dealt with the ultimate limits of chemical contributions to flame inhibition. Particular attention was focused on the inhibition cycles which regenerate the inhibitor. This lead to definition of an idealized "perfect" inhibition cycle. It was demonstrated that for such an inhibitor a stoichiometric methane/air flame additives leveled in the 0.001 – 0.01 mole percent range which resulted in a decrease in flame velocity of approximately 30%. This efficiency corresponded roughly to the observed behavior of metallic inhibitors such as iron pentacarbonyl which was known to be as much as 2 orders of magnitude more effective than currently used suppressant. This correspondence between the behavior of a "perfect inhibitor" and iron pentacarbonyl lead to the conclusion hat only gas-phase processes can account for its inhibitive power.

Rumminger and Linteris [9] showed that three CH_4-O_2-N_2 reactant mixtures was utilized with $Fe(CO)_5$ added to the fuel or oxidizer stream in each. Flame calculations that incorporated only gas-phase chemistry were used to assist in interpretation of the experimental results. In flames with the inhibitor added on the flame side of the stagnation plane, the region of particle formation overlap with the region of high H-atom concentration, and particle formation may interfere with the inhibition chemistry. When the inhibitor was added on the non-flame side of the stagnation plane, significant condensation of metal or metal oxide particles was found, and implied that particles prevented active inhibiting species from reaching the region of high radical concentration.

Alzueta et al [10] studied experimentally and theoretically the interaction of SO_2 with the radical pool under combustion conditions. The results showed that under flow-reactor conditions SO_2 may inhibit or promote oxidation of fuel, depending on conditions. In a narrow range of operating conditions close to stoichiometric SO_2 promoted oxidation through the sequence $SO_2 + H \leftrightarrow SO + OH$, $SO + O_2 \quad SO_2 + O$. Inhibition of oxidation by removal of radicals can be explained in terms of the $SO_2 + O + M$ reaction, even under fuel-rich conditions.

Thomas [11] presented the results of a computational investigation of limiting water droplet and vapor concentrations, beyond which laminar methane-air flames were incapable in self sustained propagation. The variation of laminar burning velocity with droplet size and number density have been investigated and the results were compared to analytical predictions, he concluded that the droplet of diameter 10 μm will evaporate just before the end of the exothermic reaction zone. As the droplet size increased further, increasing values of mass loading density are required. Increased efficiency of flame inhibition also was observed experimentally, and computationally when alkali salts in solutions were added to flames. The mechanism was purely chemical. The effectiveness of added salts will diminish as the mean droplet diameter increases.

Andrae et al [12] studied the wall effects in the combustion of lean methane mixtures numerically using the CHEMKIN software *(see A.1)*. Their work was to gain a deeper understanding of the flame-wall interaction in lean burn combustion, and in particular the kinetic and thermal effects, they simulated lean and steady methane-air flames in a boundary layer flow. The gas phase chemistry was modeled with the GRI mechanism version 1.2 *(see A.2)* boundary conditions included an inert wall, a recombination wall and catalytic combustion of methane. They ended with the thermal wall effects in more significant at the lower wall temperature (600K) and the wall can

essentially modeled as chemical inert for the lean mixtures used. At the higher wall temperature (1200K), the chemical wall effects were more significant and the higher the pressure (10atm) the catalytic surface retarded homogeneous combustion of methane more than the recombination wall because of product inhibition.

Mishra et al [13] tested the flammability limits of LPG-air mixture. The lower flammability limit (LFL) was found to be 1.81% and upper flammability limit (UFL) of LPG was 8.86% for upward propagation of flame, whereas, for downward propagation of flame, the LFL and UFL were 1.87 and 7.69% of LPG, respectively. The nitrogen dilution effects on the flammability limits have been explored.

Sankran and Hong IM [14] numerically studied and established the concept of dynamic flammability limit, defined as the minimum equivalence ratio above which the unsteady flame can sustain combustion. For the weak and strong strain rate cases studies. It has been observed that he dynamic flammability limit depends on the mean and frequency of the composition fluctuations. The parametric study demonstrated that the flammability limit of an unsteady premixed flame is further extended to a linear condition as the frequency or mean equivalence ratio fluctuations increases. It was also found that under all conditions, the mean equivalence ratio and the minimum flame temperature must be higher than those at the steady flammability limit to sustain combustion. It was further shown that the dynamic flammability limit is primarily determined by the instantaneous branching-termination balance at the reaction zone. The behavior of the flame response attenuation with increasing frequency was found to scale properly using the normalized frequency based on the imposed flow strain rate, which represents the characteristic time scale of the transport process within the flame.

Rumminger et al [15] presented the first data on flame inhibition by ferrocene (Fec) and showed it o be as efficient as $Fe(CO)_5$ at reducing the burning velocity of

premixed methane flames. They showed that ferrocene looses its effectiveness at a mole fraction above few hundred PPM just like iron pentacarbonyl. Experimental results implied many combinations of CO_2 and Fec showed strong inhibition, mitigating the loss of effectiveness observed for pure Fec and $Fe(CO)_5$. In contrast to the results with CO_2 Blends of CF_3H and Fec were not particularly effective, implied that iron species and halogens may enter into undesired reactions that poison the catalytic cycle.

Juchmann et al [16], investigated experimental and theoretical CH and CN radical formation and destruction in a low pressure 13.3-hPa (10 Torr) premixed stoichiometric CH_4/O_2 flame seeded with NO. The computations highlights significant differences in reaction paths and rate selection. They showed that the reaction of the CH radical with molecular oxygen is of particular importance in the present flame. The present quantitative measurements of the CN radical indicated that attention should be given to the formation and oxidation chemistry of HCN.

Vagelopoulos and Egolfopoulos [17], studied the stability of premixed flames at ultralow strain rates experimentally and numerically in the stagnation flow configuration. Direct experimental determination procedure was proposed. The proposed technique was based on the principle that whereas the planner, strained flames are positively stretched, the Bunsen flames were negatively stretched. The minimum velocity obtained in the measurements corresponded to the flame speed at the limit of near-zero stretch and is representative of the true laminar flame speed value.

Fairweather et al [18], experimentally and theoretically studied the premixed flame propagation in a number of small scale, cylindrical vessels. They found that flame propagation through the vessels, up until flame front venting, was found to be substantially laminar, with significant over pressure only being generated in the later

explosions due to rapid turbulent combustion. Mathematical model described provided a reasonable simulation of explosions within enclosures of the type investigated.

Korolchenko et al [19], measured burning velocities and flammability limits of gaseous mixtures of combustible gas (hydrogen and methane), oxidizer (oxygen and air), and diluent (nitrogen, argon, helium, carbon dioxide, steam, water aerosol formed by evaporation of superheated water) at elevated temperatures (up to 250°C) and pressures (up to 4.0 MPa). They found that with increasing temperature, the flammability region is widened for all the mixtures studied. With increasing pressure, the flammable region for mixtures of hydrogen-oxygen-diluent is narrowed, except where steam or water aerosol is the diluent. A more complicated dependence of flammability limit on pressure is found for mixtures of hydrogen-oxygen-steam. They investigated the dependences of burning velocity on temperature and pressure for stoichiometric hydrogen-air mixtures diluted by nitrogen and steam. They showed that, over the ranges of temperature and pressure considered, the temperature index of burning velocity is positive (that is, burning velocity increases with temperature), while the pressure index changes sign from positive to negative on dilution by inert agents.

Based on the forgoing literature review, it is seen that the problem of inhibitory effect of some additives on methane-air flame has not been treated in depth. All the work that was carried out so far was concerned with retarding the flame propagation, studying the wall effects on mixture combustion, water spraying as inhibitor, premixed models of mixture combustion, small scale droplet studies, radical concentration measurements, and premixed flame measurements. Until now there is little work done to investigate a suitable chemical or substance that can be used to inhibit the combustion of methane-air mixture completely from chemical kinetics control point of view. The need of such study can be covered in the present one.

Chapter Two

Combustion and Flames

2.1 Review of Combustion and Flames

Combustion can occur in either a flame or non-flame mode, and flames, in turn, are categorized as being either premixed flames or non-premixed (diffusion) flames.

The difference is obvious between the two modes. In a spark ignition engine, a premixed flame leaves combustion products behind it and as the flame moves across combustion zone the propagation occurs through combustion space. While for the non-premixed flame, rapid oxidation reaction occurs at many locations within the unburned gas leading to very rapid combustion throughout the volume called autoignition [20].

The two classes of flames, premixed and non-premixed (or diffusion), are related to the state of mixture of the reactants, as suggested by names. In a premixed flame, the fuel and oxidizer are mixed at a molecular level prior to the occurrence of any significant chemical reaction. Contrarily, in a diffusion flame, the reactants are initially separated and reaction occurs only at the interface between the fuel and the oxidizer, where mixing and reaction both take place. A simple candle is an example of a diffusion flame [20].

2.2 Stoichiometric Reaction of Methane

Because of its unique tetrahedral molecular structure with large C-H bond energies, Methane (CH_4) exhibits some unique combustion characteristics. For example, it has a higher ignition temperature, low flame speed, and is essentially unreactive in photochemical smog chemistry. Combustion of methane -major component of natural gas- is an exothermic reaction that is used mainly in major combustion processes [21].

To describe this reaction, the balanced chemical reaction equation for both stoichiometric and lean methane–air combustion can be written as [21]

$$CH_4 + \frac{2}{\phi} O_2 + \frac{7.5238}{\phi} N_2 \rightarrow CO_2 + 2H_2O + \left(2 - \frac{2}{\phi}\right) O_2 + \frac{7.5238}{\phi} N_2 \qquad (2.1)$$

To completely oxidize the fuel such that all the carbon is converted to carbon dioxide and that for hydrogen is converted to water vapor, sufficient air is required. When this condition occurs, this combustion reaction is called stoichiometric reaction. The amount of oxidizer is just enough for complete combustion to take place; thus; all the latent heat of combustion of fuel will be released at the stoichiometric air to fuel ratio.

The air-fuel ratio (AF) of combustion process is expressed in non-dimensional variable referred to as equivalence ratio Φ, i.e. the inverse of air number λ, the actual FA ratio divided by the stoichiometric FA ratio [21]:

$$\Phi = \frac{1}{\lambda} = \frac{(Fuel/Oxidizer)_{actual}}{(Fuel/Oxidizer)_{stoich}} \qquad (2.2)$$

Fuel system may be rich, less oxidized for $\Phi > 1$, lean, more oxidized for $\Phi < 1$, or as stated stoichiometric for $\Phi = 1$. At lower than stoichiometric value the oxygen deficiency is the case, and incomplete combustion with partially burned fuel, produces carbon monoxide and unburned hydrocarbons, which will escape from combustion zone.

2.3 Flame Temperature

The rate of chemical reaction is controlled by the flame temperature. At equilibrium, reactants and products energy balance determines the flame temperature. When a thin reaction zone compared to the rest of the range of interest exists, the maximum temperature in the reaction zone is denoted as the flame temperature. From

thermodynamics, if the combustion process occurs adiabatically, no work, no changes in the kinetic or potential energy, then flame temperature is called adiabatic flame temperature. Reactants can achieve this maximum temperature because any heat transfer from the reaction zone and any incomplete combustion would lower the products temperature [21].

The important factors affecting adiabatic flame temperature are initial temperature of air, pressure, AF ratio and type of fuel. The dissociation effects play an important role in order that the adiabatic flame temperature reaches its maximum value. Therefore, the adiabatic flame temperature depends strongly on the AF ratio besides stoichiometric. In lean region, heat loss is increased due to increased excess air. In rich region, incomplete combustion due to insufficient air and flame temperature decreases [21].

An increase in the flame temperature is a result of the increase in the initial temperature. This leads to anticipated storage of additional energy in dissociated species form, as an incomplete combustion case. The adiabatic temperature can be calculated from a known AF relation as [21],

$$T_{adiab}(K) = Exp\left[9.1418 - \left(\frac{1.4727}{\lambda}\right) - 1.6161 * \ln\lambda\right] \qquad (2.3)$$

Where, λ: is the inverse of the air number.

Equation 2.3 and Fig. 2.1 are comparative results for methane flame. It is noted that the maximum flame temperature is achieved at lean-than-stoichiometric mixtures. The simplest explanation for this behavior is the absence of several losses due to dissociation and variable specific heats.

The effect of initial air temperature can be observed in Fig. 2.2 and Equation 2.4 for different values of air temperature [21].

$$T_{adiab}(K) = 2087.2 + 0.46502 * T_i(K) \quad (2.4)$$

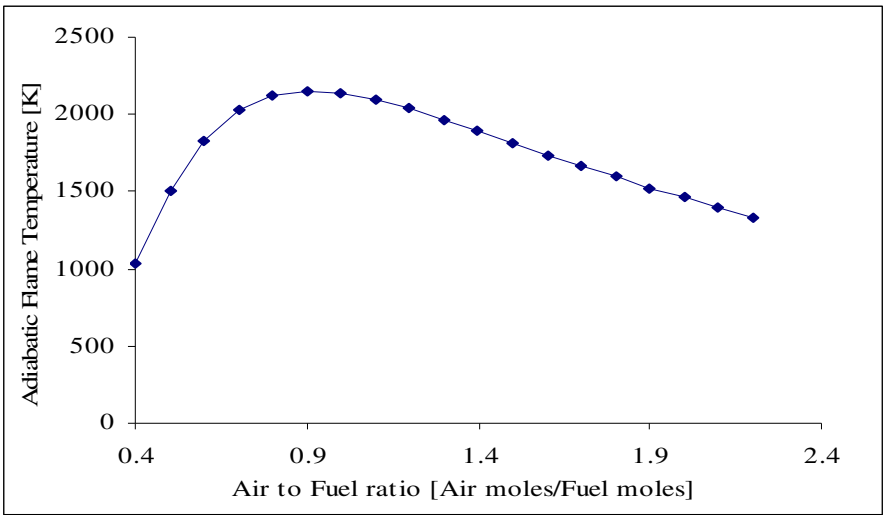

Figure 2.1 Distribution of the methane adiabatic flame temperature against AF at ambient pressure and temperature [21].

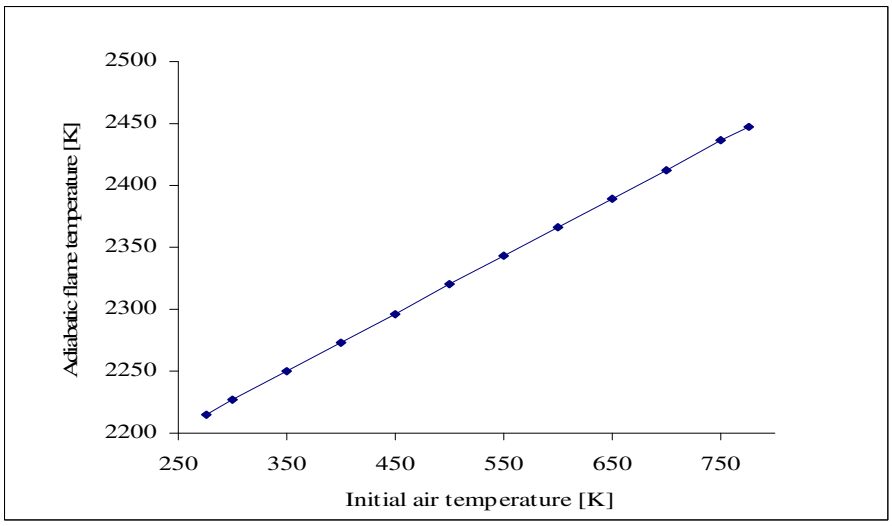

Figure 2.2 Distribution of methane adiabatic flame temperature against initial air temperature at ambient pressure and stoichiometric air-fuel ratio [21].

A weak correlation between flame temperature and pressure is an established fact. The effect of pressure on the adiabatic flame temperature at stoichiometric conditions and ambient initial air temperature is shown in Equation 2.5 which is fitted

between adiabatic flame temperature and pressure. As shown in Fig. 2.3, a 30 bar increase in pressure caused an increase of only 50˚C in temperature [21].

$$T_{adiab}(K) = \frac{1407.7 + 2314.2 * p(atm)^{0.39908}}{0.67297 + p(atm)^{0.39908}} \quad (2.5)$$

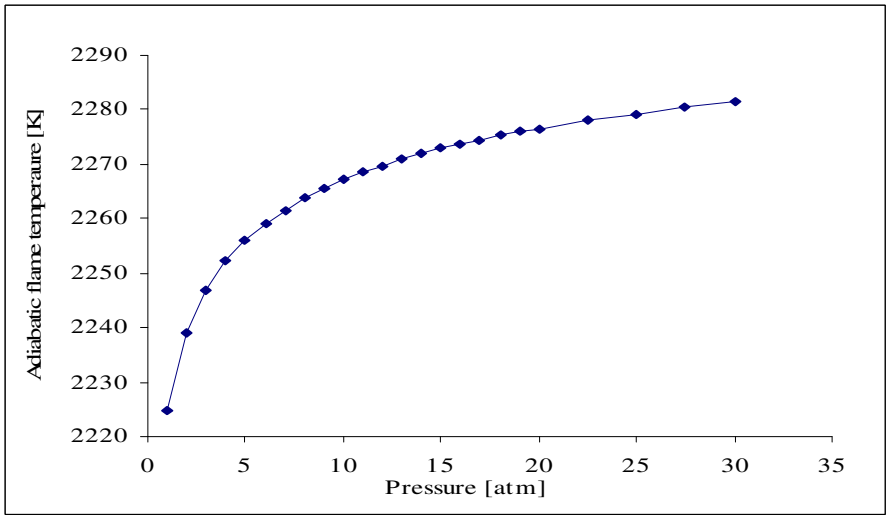

Figure 2.3 Distribution of methane adiabatic flame temperature against pressure at ambient temperature and stoichiometric conditions [21]

Hydrocarbon air mixtures maximum temperature lies between 2200-2400 K, and for mixtures with oxygen the temperature varies between 3000-4000K. The "laminar flame theory" [20] states that the flame temperature has a substantial effect on the laminar flame speed. The flame temperature determines the flame speed and influences the combustion products formed. The concentration of carbon monoxide (CO) and Nitrogen oxides (NO_x) are pollutants that depend on the flame temperature.

2.4 Laminar Flame Speed

The laminar flame speed (burning velocity, normal combustion velocity, and flame velocity) is defined as the speed at which premixed (unburned) gases across the combustion zone (wave) normal in direction to the surface of the wave.

Flame speed is an important property because of its usefulness according to the followings: predicting the actual burning fuel rate, validation of chemical reaction mechanism, and finally, turbulent flame calculations are based on laminar flame speed. This speed is affected with the followings: fuel, AF ratio, temperature and pressure.

The laminar flame speed behavior was studied by researchers according to pressure and initial temperature effects [25-35]. The measurement of laminar flame speed of stoichiometric methane–air premixed flame covering distribution of both initial temperature and pressure was investigated by Garforth and Rallis [25]. Toshio and Takeno [26] studied the pressure and temperature effects on laminar flame speed for hydrogen-air flame and methane-air mixtures with the use of a spherical bomb technique. Flame theory states that the pressure effect can be related to order of reaction with following form [21]

$$S_L \alpha p^{(n-2)/2} \tag{2.6}$$

Then, with (n=2), the case of bimolecular reactions, independent laminar flame speed with pressure. Therefore, general experimental measurements obtain a negative distribution for laminar flame speed against pressure. Andrews and Bradley [28] found following speed to pressure relation [21]

$$S_L(cm/s) = 43[p(atm)]^{-0.5} \tag{2.7}$$

This correlation can be used for laminar flame speed pressure distribution for a stoichiometric methane-air mixture with more than 5 bar pressure.

Another expression can serve in simulating flame speed as inversely proportional to pressure distribution at ambient temperature and stoichiometric AF ratio is the following [21]

$$S_L(cm/s) = 48.128 * [p(atm) + 0.7912]^{-0.51394} \tag{2.8}$$

Experimentally and numerically, it was found that an increase in initial temperature will increase flame speed.

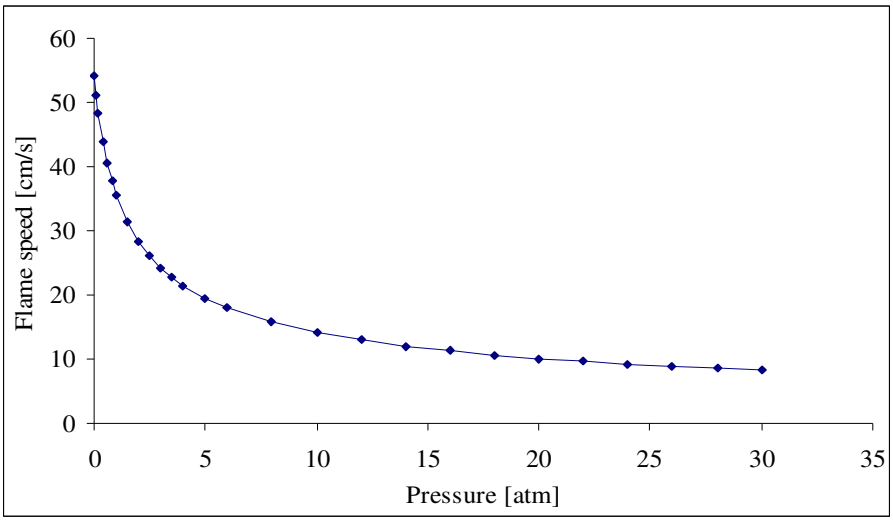

Figure 2.4 Distribution of methane flame speed against pressure at ambient temperature and stoichiometric AF ratio [21].

Dugger [33, 34] gives an idea about the dependence of flame speed on initial temperature for three mixtures, methane-air, propane-air, and ethylene-air mixture. Results was increasing of flame speed with initial temperature, and could be reproduced using an equation of the form [21]

$$S_L(cm/s) = b + cT_i^n \tag{2.9}$$

Where b, c, and n are fuel constants specified for a given fuel.

An experimental study by Metghalchi and Keck [35] ended with an empirical formula obtained for stoichiometric methane-air flame speed over temperature ranging from 141 to 617 K. in the equation b = 8, c = 27, and n = 2.11 [35]

$$S_L(cm/s) = 8 + 27\left(\frac{T_i(K)}{T_o(K)}\right)^{2.11} \tag{2.10}$$

Fig. 2.5 shows results for Horel Model formula [35]

$$S_L(cm/s) = 0.228 * (1.0022^{T(K)}) * T_i(K)^{0.79719} \tag{2.11}$$

Changes of AF ratio will affect the laminar flame speed due to changes in temperature with the mixing ratio.

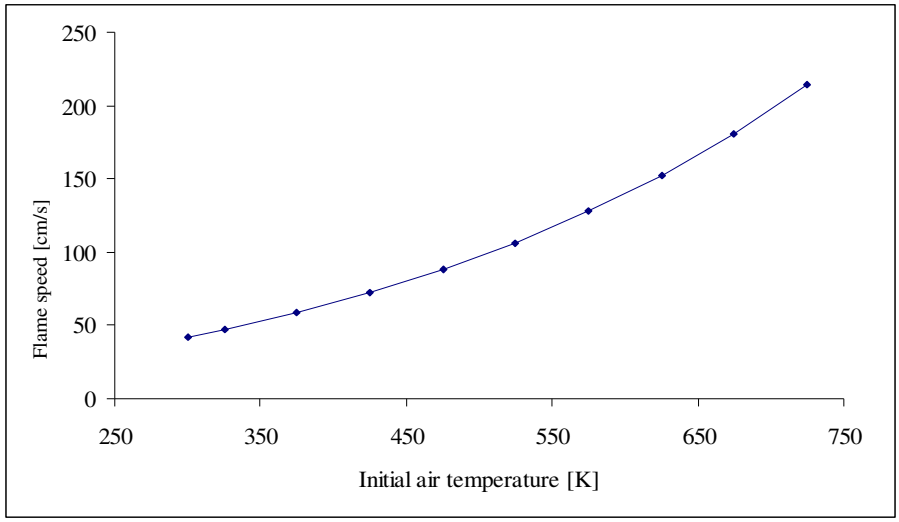

Figure 2.5 Distribution of methane flame speed against inlet air temperature at ambient pressure and stoichiometric AF ratio [21]

Unless very rich mixtures, the major effect of equivalence ratio on flame speed for similar fuels is a result of the effect of this parameter on flame temperatures. Thus the peak speed of hydrocarbon fuels flames occurs at stoichiometric or slightly fuel rich-mixtures.

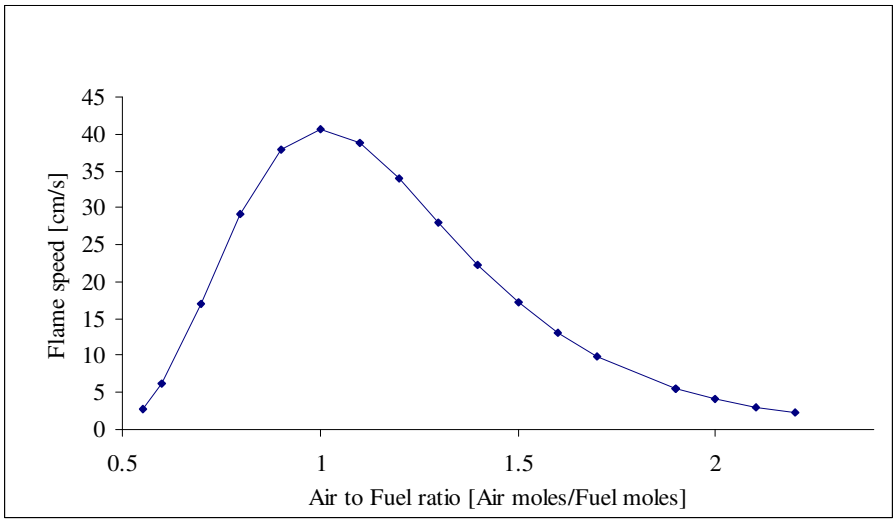

Figure 2.6: Distribution of methane flame speed against AF ratio at ambient pressure and temperature [21]

The flame speed is plotted against AF ratio for methane at ambient pressure and temperature through the formula in Fig. 2.6 [21].

$$S_L(cm/s) = Exp\left[15.739 - \left(\frac{12.033}{\lambda}\right) - 11.997 * \ln\lambda\right] \quad (2.12)$$

The Bunsen-burner flame provides an interesting example of laminar premixed flames. A jet of fuel at the base induces a flow of air through the variable area port, and the air and fuel mix as the they flow up through the tube. The shape of the flame is determined by he combined effects of the velocity profile and heat losses to the tube wall. For the flame o remain stationary, the flame speed must equal the speed of the normal component of unburned gas a each location, resulting in conical shape of flame front [3].

One dimensional flat flames are frequently studied in the laboratory and are also used in some radiant heating burners. In an adiabatic burner, a flame is stabilized over a bundle of small tubes through which the fuel-air mixture passes laminarly. Over a narrower range of conditions, as flat flame is produced. The non-adiabatic burner utilizes a water-cooled face that allows heat to be extracted from flame, which, in turn, decreases the flame speed, allowing flames to stabilized over relatively wide range of flow conditions [3].

2.5 Flames Classifications

Flames can be classified in several ways, depending on how the oxidizer and the fuel reach the reaction front. Flames can be classified into three types, diffusion, premixed and partially premixed flames.

This is based on if the fuel and air are mixed prior to combustion or mixed by diffusion in the flame zone. Based on the prevailing flow velocities, these types of flames can be further classified as laminar or turbulent. Reaction zone nature is used to

divide flames into near a well-stirred reactor, a plug flow reactor or a wrinkled laminar flamelet [21]. The fuel and oxidizer, in non-premixed flames, are present on either side of the reaction zone. They are brought to the reaction zone in an unmixed state primarily due to diffusion of reactants into, the product out of the reaction zone.

In such flames, the reaction zone is established ideally at a location where the mixing leads to stoichiometric conditions, thereby producing the maximum possible flame temperature for a given combination of reactant species [21].

The fuel and oxidizer, in the fully premixed, are thoroughly mixed prior to reaching the reaction zone, also known as the flame front. The diffusion of reactants is not defining the position of the reaction zone, but balancing the local convective velocity of the reactants with the rate of consumption of the reactants popularly known as the flame speed. Based on the stabilized method, fully premixed flames could be burned at equivalence ratios other than 1. Thus, lower flame temperatures can be achieved [21].

The fuel is injected into the oxidizer flow, in the partially premixed flames, just upstream of the flame. Under such conditions, there is no enough time for the fuel and oxidizer to mix thoroughly and thus, concentration gradients across the flow are generated in the reactant stream which enters the flame front.

These flames are neither purely non-premixed, nor are fully premixed, hence, they are termed as partially premixed. Such flames are characterized by their degree of unmixedness, which is a measure of how much the radial concentration profiles of the flow deviate from a fully premixed case [21].

2.6 Structure of Premixed Flame

Fig. 2.7 shows the inner structure of a laminar, stationary, stoichiometric methane-air flame obtained by the analysis that is based on the detailed reaction

mechanism, GRI-Mech* [36], which consist of 325 elementary chemical reactions. Three characteristic zones are identified as: the chemically inert preheat zone, the inner layer, and the oxidation zone.

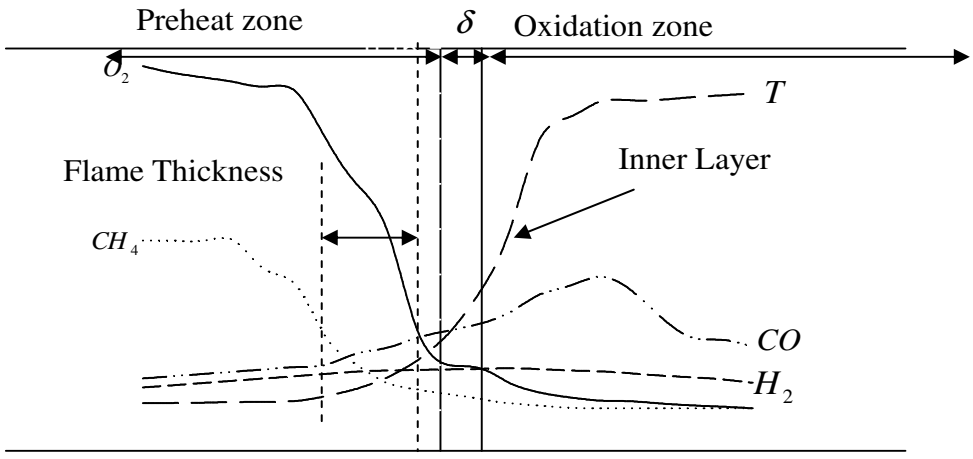

Figure 2.7 Calculated inner structure of a laminar, stoichiometric, methane-air flame [1].

Unburned gas approaching the stationary flame structure with velocity S_L is first preheated in a chemically inert zone, called preheat zone.

Here, a balance between convection and diffusion exists. In the inner zone, all the hydrocarbon chemistry occurs resulting in the formation of H_2 and CO [1].

How an element of the flowing gas can receive heat? The answer is: either chemical reactions occurring within it, or by conduction from the hotter gas ahead of it.

The chemical reactions occur in a thin layer, called inner layer [37], where the fuel is consumed. A diffusive reacting balance exists.

The inner layer is characterized by the inner layer temperature T_i, which corresponds to the cross-over temperature between chain branching and chain breaking reactions [38].

The inner layer temperature is T_i = 1370K, for stoichiometric methane-air flames at ambient pressure [38].

If the inner layer remains intact, this is a must condition for combustion process to be sustained.

If enhanced transport of heat and radicals out of the inner layer exceeds their production in the inner layer, then the reactions in the inner layer may breakdown, thus extinguishing the flame.

Downstream of the inner layer is a broader but still asymptotically thin H_2-CO oxidation layer. Here, primarily CO and H_2 oxidize to form CO_2 and H_2O.

2.7 Flammability Limits

Flammability limits, also called flammable limits, or explosive limits give the proportion of combustible gases in a mixture, between which limits this mixture is flammable.

Gas mixtures consisting of combustible, oxidizing, and inert gases are only flammable under certain conditions.

The lower flammable limit (LFL) (lower explosive limit) describes the leanest mixture that is still flammable, i.e. the mixture with the smallest fraction of combustible gas, while the upper flammable limit (UFL) (upper explosive limit) gives the richest flammable mixture. Increasing the fraction of inert gases in a mixture raises the LFL and decreases UFL [39].

To explain the concept of flammability let us take ethane (C_2H_6) as an example. Ethane will not burn in ethane air mixture until 3% of ethane is reached, below this percent ethane will not burn, so that 3% is called lower flammability limit or lean limit.

And if the proportion of ethane is increased, the combustion would become easier until 12.4% is reached, where above this percent the mixture will not burn; therefore 12.4% is called upper flammability limit or rich limit.

The lower and upper explosion concentration limits for some common gases are indicated in Table 2.1. Some of the gases are commonly used as fuel in combustion processes, *(also see A.3)* [40].

Table 2.1: Lower and upper flammability limits of some fuel gases indicated for gas and air at $20^{o}C$ and atmospheric pressure. [40]

Fuel Gas	"Lower Explosive or Flammable Limit" (LEL/LFL) (%)	"Upper Explosive or Flammable Limit" (UEL/UFL) (%)
Benzene	1.35	6.65
n-Butane	1.86	8.41
iso-Butane	1.80	8.44
iso-Butene	1.8	9.0
Butylene	1.98	9.65
Cyclohexane	1.3	8
Cyclopropane	2.4	10.4
Diethyl Ether	1.9	36
Ethane	3	12.4
Ethylene	2.75	28.6
Ethyl Alcohol	3.3	19
Hydrogen	4	75
Isobutane	1.8	9.6

The UFL increases with increasing initial pressure, initial temperature and hydrogen fuel concentration. The LFL decreases slightly as pressure is increased.

However, the UFL can increase or decrease depending upon the fuel, but for hydrogen and hydrocarbon the UFL is increased as pressure increased [41].

For an upward propagating flame, the upward convection of the hot products tends to help the flame propagate and thus upward propagation gives slightly wider limits than either downward or horizontal propagation [42].

Increasing the initial mixture temperature will widen the flammability limits range, this is because increasing initial mixture temperature will help diffusion of the ignition source in propagation of the flame and enable mixture to propagate [32].

Auto ignition temperature is the lowest temperature of a hot wall adjacent to the fuel-air mixture which can lead to ignition without any ignition source [40]. Auto ignition temperature for methane-air mixture is 630ºC [43].

2.8 Inhibitors and Retardants

Flame inhibitors are materials that retard or resist the spread of fire. These can be separated into several categories [44]:

- Minerals such as asbestos, compounds such as aluminum hydroxide, magnesium hydroxide, antimony trioxide, various hydrates, red phosphorus, and boron compounds, mostly borates.
- Tetrakis (hydroxymethyl) phosphonium salts, made by passing phosphate gas through a solution of formaldehyde and a mineral acid such as hydrochloric acid, are used as flame retardants for textiles.
- Synthetic materials, usually halocarbons.

Halogenated hydrocarbons are known to be good inhibitors for methane-air and hydrogen-air flames by measure flammability limit and burning velocity [45], these studies showed that bromine and iodine compounds are the most efficient flame

suppressant. But because of its bad affects on the ozone depletion, (Montreal Protocol, 1990) their use being limited.

The search for effective replacements for halogenated hydrocarbons resulted in the discovery of several promising materials like organophosphorus compounds [46] and solid aerosols (sodium bicarbonate ($NaHC0_3$) and potassium bicarbonate ($KHCO_3$) powders) [47].

Organophosphorus and solid aerosols materials was found to have a good effect in reducing the burning velocity and inhibiting the flame propagation. Fig. 2.8 shows comparison between several suggested inhibitors e.g. CO_2, CF_3Br, $Sn(CH_3)_4$, $SnCl_4$, MMT, TMP and $Fe(CO)_5$.

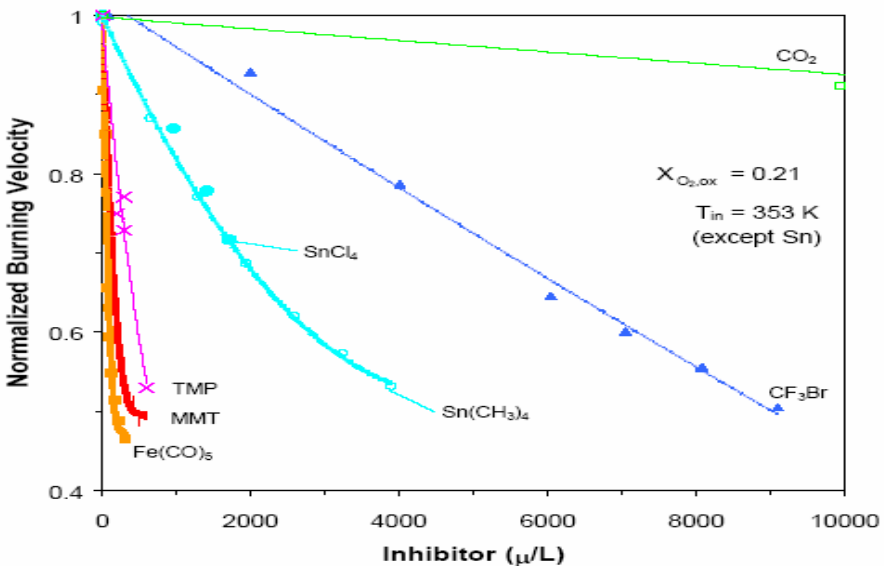

Figure 2.8: Normalized burning velocity of premixed $CH_4/O_2/N_2$ flames inhibited by CO_2, CF_3Br, $Sn(CH_3)_4$, $SnCl_4$, MMT, TMP, and $Fe(CO)_5$ (T_{in} = 353 K for all data except $Sn(CH_3)_4$ and $SnCl_4$ which are at 298 K). Lines are curve fits to data[48].

Based on burning velocity of premixed $CH_4/O_2/N_2$ flames, the figure shows that metallic compounds like $Fe(CO)_5$ is the most effective inhibitor in a low volume fraction [48].

This is an extremely important factor in the selection of any inhibitor i.e. to have maximum inhibition effect with least concentrations.

2.9 Theoretical Model and Algorithm

The equations governing steady, isobaric, quasi-one-dimensional flame propagation are discussed in this section. These equations are applicable to the following two main models:

1. Premixed Laminar Burner-stabilized Flame
2. Premixed Laminar Flame-speed Calculation

Many practical combustors, such as internal combustion engines, rely on premixed flame propagation. Moreover, burner-stabilized laminar premixed flames are often used to study chemical kinetics in a combustion environment.

Such flames are effectively one-dimensional and can be made very steady, facilitating detailed experimental measurements of temperature and species profiles.

Also, laminar flame speed is often used to characterize the combustion of various fuel-oxidizer combinations and in determining mixture flammability limits.

Therefore, the ability to model chemical kinetics and transport processes in these flames is critical to flammability studies, interpreting flame experiments, and to understanding the combustion process itself.

The Premixed Flame Models solve the set of governing differential equations that describe the flame dynamics using implicit finite difference methods, as well as, a combination of time-dependent and steady-state methods.

The solver algorithm employed automates coarse-to-fine grid refinement as a means to enhance the convergence properties of the steady-state approach and as a means to provide optimal mesh placement.

Numerical simulations of laminar premixed flames employing both detailed chemical kinetics and mixture transport properties have become standard tools for combustion engineers and scientists. Many simulations are based on libraries of FORTRAN main programs and subroutines.

2.9.1 Governing Equations

The basic conservation equations describing steady, one-dimensional flames [3]:

- Continuity Equation

$$\frac{d\dot{m}''}{dx} = 0 \tag{2.13}$$

- Species Conservation Equation

$$\dot{m}''\frac{dY_i}{dx} + \frac{d}{dx}\left(\rho Y_i V_{i,diff}\right) = \dot{\omega}_i MW_i \quad \text{for i = 1,2, … , N species,} \tag{2.14}$$

- Energy Conservation Equation

$$\dot{m}'' c_p \frac{dT}{dx} + \frac{dT}{dx}\left(-k\frac{dT}{dx}\right) + \sum_{i=1}^{N} \rho Y_i V_{i,diff} C_{p,i}\frac{dT}{dx} = -\sum_{i=1}^{N} h_i \dot{\omega}_i MW_i \tag{2.15}$$

- Moment Conservation Equation

Not explicitly required since pressure is assumed to be constant, as a simplified flame analysis.

In addition to these conservation equations, the following ancillary relations or data are required [3]:

- Ideal-gas equations of state.
- Constitutive relations for diffusion velocities,

  $v_{i,diff,X} = -\frac{D_{im}}{Y_i}\nabla Y_i$ i = 1,2, … N-1, D_{im} is the effective binary diffusion coefficient for species *i* in he mixture *m*.

- Temperature dependent species properties, $h_i(T)$, $C_{p,i}(T)$, $k_i(T)$, *and* $D_{ij}(T)$.

- Mixture property relations to calculate MW_{mix}, k, D_{ij},, and D_i^T from individual species properties and mole (or mass) fractions.
- A detailed chemical kinetic mechanism to obtain the $\dot{\omega}_i s$.
- Interconversion relations for mole fractions and mass fractions.

2.9.2 Boundary Conditions

The conservation equations (2.13), (2.14), and (2.15) described a boundary value problem; i.e., given information about the unknown functions (T, Y_i) at an upstream location (boundary) and a downstream location (boundary), the problem is to determine $T(x)$ and $Y_i(x)$ between these two boundaries.

Assuming attached coordinate system to the flame (freely propagation). Equation (2.15) is simply, and clearly, second-order in only T and, thus, requires two boundary conditions [3]:

$$T(x \to -\infty) = T_u \qquad \text{and} \quad \frac{dT}{dx}(x \to +\infty) = 0 \tag{2.16}$$

Considering equation (2.14) to be second order in Y_i, appropriate conditions are that the $Y_{i,s}$ are known values for the upstream and that the mass-fraction gradients become vanishingly small far downstream [3]:

$$Y_i(x \to -\infty) = Y_{i,O} \text{ and } \frac{dY_i}{dx}(x \to +\infty) = 0. \tag{2.17}$$

And for the freely propagation case, one explicitly fixes the coordinate system to move with the flame [3]:

$$T(x_1) = T_1 \tag{2.18}$$

The net chemical production rate of each species results from a competition between all the chemical reactions involving that species.

It is presumed that each reaction proceeds according to the law of mass action and the forward rate coefficients are in the modified Arrhenius form [36]:

$$k_f = AT^{\beta} \exp\left(\frac{-E_A}{RT}\right) \tag{2.19}$$

where A: Arrhenius constant, T: Temperature, E_A: is activation energy, R: Gas Constant.

In addition to chemical reaction rates, one must also be concerned with the transport properties of the species, i.e., thermal conductivities and diffusion coefficients. Stockmayer potentials are used throughout in evaluating transport properties.

The user has the option of evaluating transport properties using mixture-averaged formulas or a multi-component diffusion model.

2.9.3 Algorithm Structure and Modification

To implement these equations in a simulation software, following algorithm describes the needed strategy in developing the simulation software.

To initialize the species and reaction specific information, the algorithm makes appropriate calls to the gas phase and transport libraries.

After reading of linking files, required spaces are stored for processing the subroutines.

The algorithm Fig. 2.9 then reads any other needed input parameters like flame temperature profile, and begins its iteration from previously computed flame solution. The output is then produced, and the solution file can be used to restart the algorithm, this file is also a save file.

The first modification was related to the initial gas phase chemistry file, thermodynamics data file, and transport data file. By modifying the chemical reactions and finding related properties.

The next change in the algorithm was related to initial conditions and geometry of apparatus used. By introducing the detailed geometry and conditions available.

The final change was related to solution file, in order to get an optimum solution for the iterated outputs. By editing the final iterative solution to export final output.

The used GRI-Mech. was similar to the one shown in Fig. 2.10 Below.

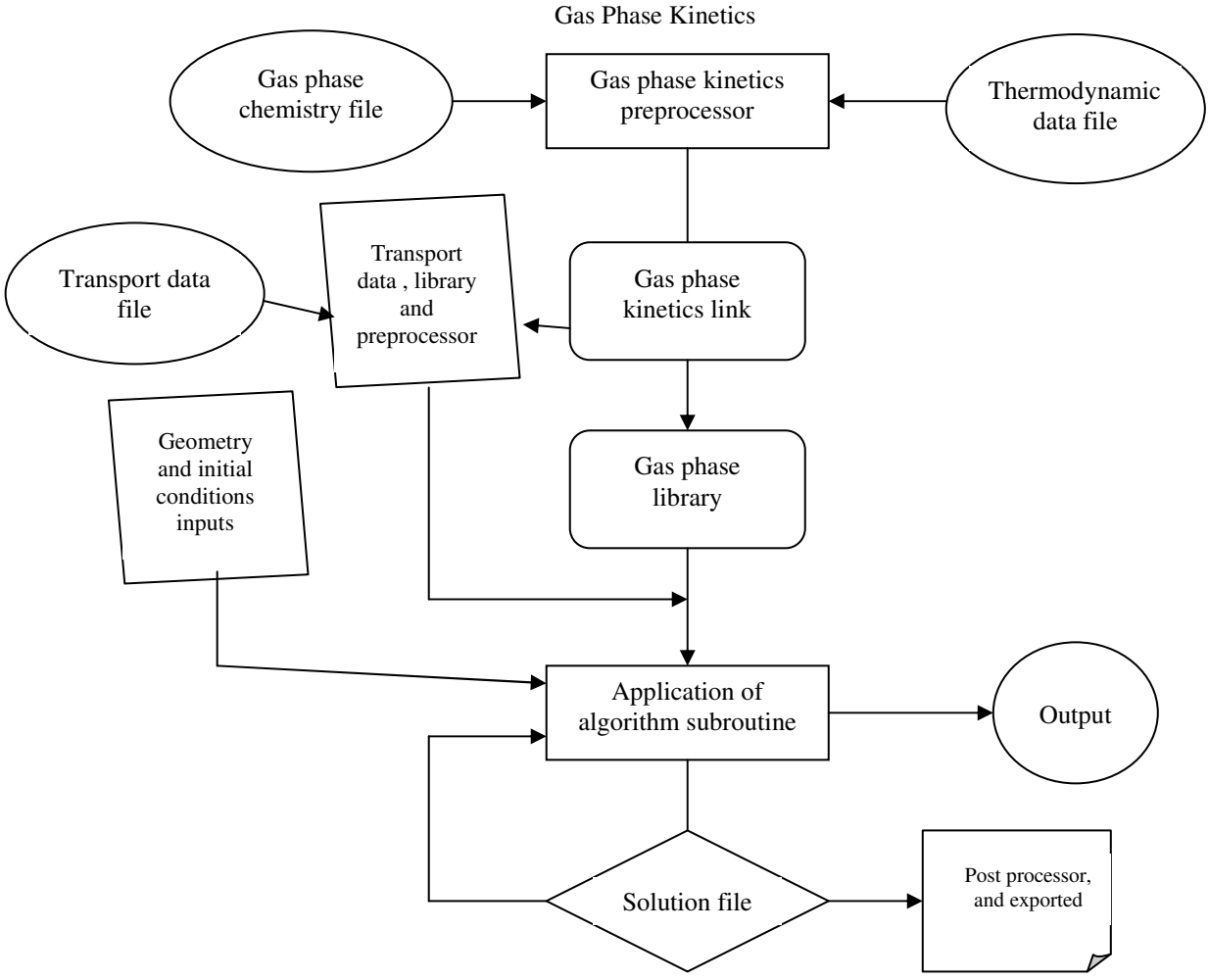

Figure 2.9 Algorithm of modified software with developed data files and processors

```
ELEMENTS   H   O    C   N END
SPECIES    CH4 CH3 CH2 CH CH2O HCO CO2 CO H2 H O2 O OH HO2 H2O2 H2O N2
END
REACTIONS
CH3+H+M=CH4+M              8.0E26     -3.        0.
CH4+O2=CH3+HO2             7.9E13      0.    56000.
CH4+H=CH3+H2               2.2E4       3.     8750.
CH4+O=CH3+OH               1.6E6       2.36   7400.
CH4+OH=CH3+H2O             1.6E6       2.1    2460.
CH3+O=CH2O+H               6.8E13      0.        0.
CH3+OH=CH2O+H2             1.0E12      0.        0.
CH3+OH=CH2+H2O             1.5E13      0.     5000.
CH3+H=CH2+H2               9.0E13      0.    15100.
CH2+H=CH+H2                1.4E19     -2.        0.
CH2+OH=CH2O+H              2.5E13      0.        0.
CH2+OH=CH+H2O              4.5E13      0.     3000.
CH+O2=HCO+O                3.3E13      0.        0.
CH+O=CO+H                  5.7E13      0.        0.
CH+OH=HCO+H                3.0E13      0.        0.
CH+CO2=HCO+CO              3.4E12      0.      690.
CH2+CO2=CH2O+CO            1.1E11      0.     1000.
CH2+O=CO+H+H               3.0E13      0.        0.
CH2+O=CO+H2                5.0E13      0.        0.
CH2+O2=CO2+H+H             1.6E12      0.     1000.
CH2+O2=CH2O+O              5.0E13      0.     9000.
CH2+O2=CO2+H2              6.9E11      0.      500.
CH2+O2=CO+H2O              1.9E10      0.    -1000.
CH2+O2=CO+OH+H             8.6E10      0.     -500.
CH2+O2=HCO+OH              4.3E10      0.     -500.
CH2O+OH=HCO+H2O            3.43E9      1.18   -447.
CH2O+H=HCO+H2              2.19E8      1.77   3000.
CH2O+M=HCO+H+M             3.31E16     0.    81000.
CH2O+O=HCO+OH              1.81E13     0.     3082.
HCO+OH=CO+H2O              5.0E12      0.        0.
HCO+M=H+CO+M               1.6E14      0.    14700.
HCO+H=CO+H2                4.0E13      0.        0.
HCO+O=CO2+H                1.0E13      0.        0.
HCO+O2=HO2+CO              3.3E13     -0.4       0.
CO+O+M=CO2+M               3.2E13      0.    -4200.
CO+OH=CO2+H                1.51E7      1.3    -758.
CO+O2=CO2+O                1.6E13      0.    41000.
HO2+CO=CO2+OH              5.8E13      0.    22934.
H2+O2=2OH                  1.7E13      0.    47780.
OH+H2=H2O+H                1.17E9      1.3    3626.
H+O2=OH+O                  5.13E16    -0.816 16507.
O+H2=OH+H                  1.8E10      1.0    8826.
H+O2+M=HO2+M               3.61E17    -0.72      0.
H2O/18.6/  CO2/4.2/  H2/2.86/  CO/2.11/  N2/1.26/
OH+HO2=H2O+O2              7.5E12      0.        0.
H+HO2=2OH                  1.4E14      0.     1073.
2OH=O+H2O                  6.0E8       1.3       0.
H+H+M=H2+M                 1.0E18     -1.0       0.
H+H+H2=H2+H2               9.2E16     -0.6       0.
H+H+H2O=H2+H2O             6.0E19     -1.25      0.
H+H+CO2=H2+CO2             5.49E20    -2.0       0.
H+OH+M=H2O+M               1.6E22     -2.0       0.
H+O+M=OH+M                 6.2E16     -0.6       0.
H+HO2=H2+O2                1.25E13     0.        0.
HO2+HO2=H2O2+O2            2.0E12      0.        0.
H2O2+M=OH+OH+M             1.3E17      0.    45500.
H2O2+H=HO2+H2              1.6E12      0.     3800.
H2O2+OH=H2O+HO2            1.0E13      0.     1800.
END
```

Figure 2.10 Copy of GRI-Mech used in modeling and simulation.

Chapter Three

Experimentation and Data Observation

This chapter discusses the experimental procedure followed for data observation in this experimental work.

3.1 Experimental Setup

The setup used in this experiment is shown in Fig. 3.1 as shown below.

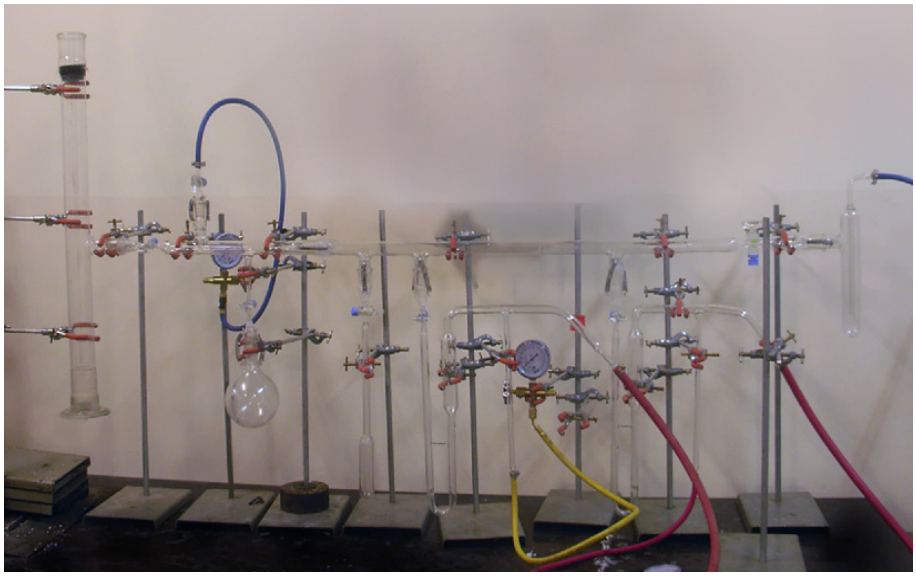

Figure 3.1: Picture of experimental setup used.

The apparatus consisted of two main components:

I. Glasswork component

A complete experimental setup made of pyrex glass was built. A set of cock valves and fittings were installed to control the flow and other operations like evacuation and mixing. The inlet sections along with the mixing part were put in a horizontal manner as shown in the figure.

The vertical section consisted of the ignition tube and was located at one end of the horizontal section. On the other side of the horizontal section, a vacuum pump was located to evacuate and flush the system after each run.

These features of the parts used in this setup are as follows:

- Ignition tube, which has 0.05 m diameter and 1 m length in a vertical position.
- A horizontal cylindrical Pyrex tube, which has 0.03 m diameter and 2 meter length, which is used to connect the parts of the apparatus.
- Entrance of the gasses in the horizontal tube. Each entrance has a cock valve to avoid leakage during the experiment.
- A pressure gauge was used to measure the partial pressure of gasses. The gas maximum pressure was 1 atm.
- Pressure gauges were also equipped at inlets of gases, vacuum pump, and ignition tube Fig. 3.2.

Figure 3.2: Picture of some pressure gauges used in the apparatus.

- Tubes to connect the cylinders, vacuum pump, and air compressor with the apparatus.
- Three types of gases (Methane, CO_2, and N_2) in addition to air were used in the experiment.
- A vacuum pump to evacuate the system before a new test, see Fig. 3.3.

Figure 3.3: Picture of vacuum pump used in experimental setup.

- An electric igniter placed at the bottom of the ignition tube.

II. Flame speed measurement parts:

The following parts where used to measure the flame speed:

- Four photoelectric cells were placed at equal distances along the ignition tube at a wooden stand, Fig. 3.4.

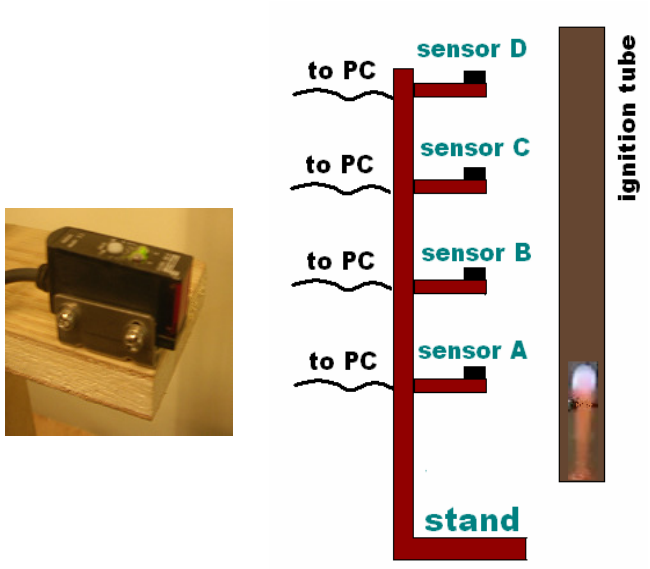

Figure 3.4: Picture for photovoltaic cell and connection to a wooden stand.

- A PLC – this was programmed and flame speed software also was designed to use in finding the time of moving flame through the ignition tube - connected to the four photoelectric cells, and also connected to a computer to display the measurement.
- A high-speed camera which was used to view the flame. Due to certain limitations on the operation and the number of frames available, it could not be used for speed measurements.

3.1.1 Flame Speed Measurements

The flame speed is the measured rate of expansion of the flame front in a combustion reaction. Whereas flame speed is generally used for a fuel, a related term is

explosive velocity, which is the same relationship measured for an explosive. Combustion engineers differentiate between the laminar and turbulent flame speeds [40]. It was found that as the fuel gas mixture approaches either limits of flammability burning velocity will be reduced [45]. To illustrate this, consider Fig. 3.5, which is a plot of burning velocity with the composition gaseous mixture on a volume basis v/v, [41].

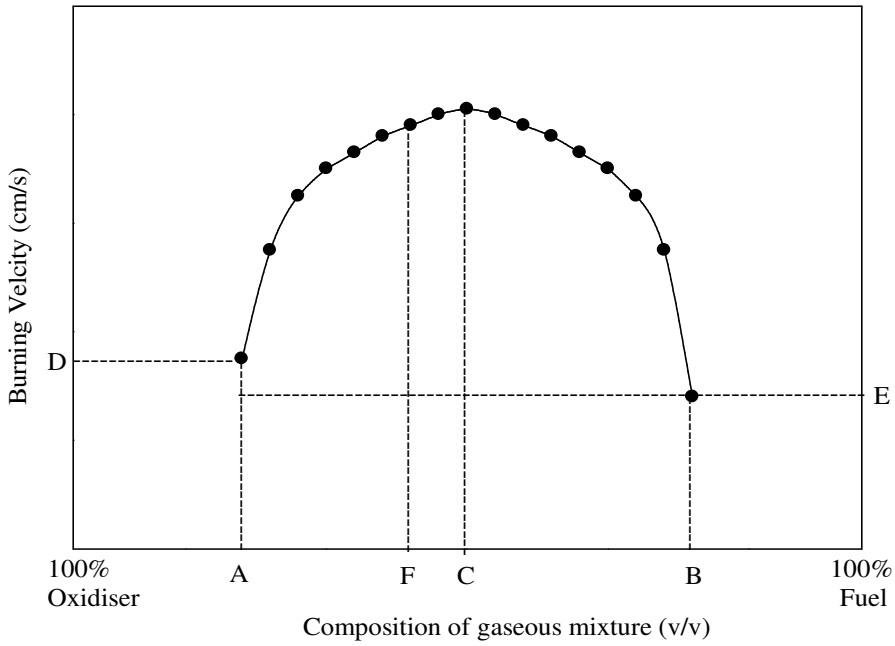

Figure 3.5: Illustrated drawing for flammability limits with burning velocity [41].

Point A: Lower flammability limit.

Point B: Upper flammability limit.

Point C: Composition of mixture with maximum burning velocity.

Point D: Burning velocity at lean limit.

Point E: Burning velocity at rich limit.

Point F: Stoichiometric point for the mixture concerned.

The Stoichiometric composition is defined as the composition where the amounts of fuel and oxygen (air) are in balance so that there is no excess of fuel or oxygen after the chemical reaction has been completed.

From Fig. 3.5, it is noted that values of burning velocities at each limits of flammability are not necessarily to be equal [41].

Flame speed is an experimentally determined property characterizing the propagation velocity of the flame normal to the flame front into the reactants. Table 3.1 shows a subset of flame speed data.

Table 3.1: Laminar flame speeds for various pure fuels burning in air at stoichiometric composition and standard temperature and pressure [3].

Fuel	Formula	Laminar Flame Speed (cm/s)
Methane	CH_4	40
Acetylene	C_2H_2	136
Ethylene	C_2H_4	67
Ethane	C_2H_6	43
Propane	C_3H_8	44
Hydrogen	H_2	210

3.1.2 Some Methods for Flame Speed Measurements

In practice, flame speed measured by using four sensors located along the ignition tube at equal and known distances.

These sensors are running like a switch, when the flame passes through the first sensor it switches a timer on, and then when it reaches the second sensor it switches it off.

At the same time the second timer is switched on for a new distance, and it continues until the flame reaches the fourth sensor which will turn off the third timer.

So, three velocities can be taken from the four sensors, and the average will represent flame speed. Fig. 3.6 shows photo for the interface of the computer program used with sensors.

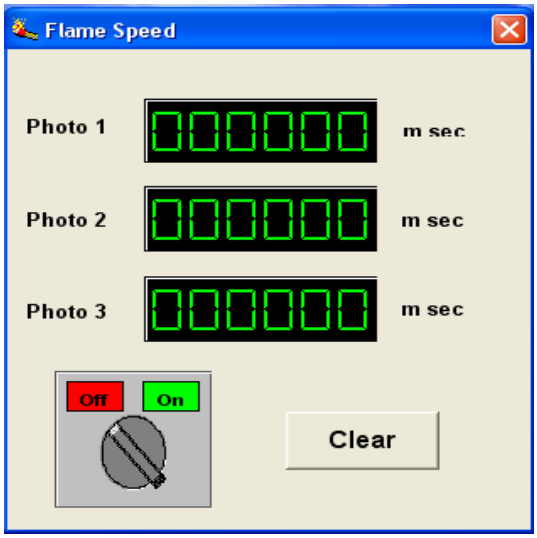

Figure 3.6: Photo of the software flame speed interface.

To calculate flame speed from photovoltaic cell: The time needed to travel 13.5 cm is 0.3535 second.

So the flame speed is calculated as; S_L = (0.135/0.3535 = 38.2 cms^{-1}).

A high speed camera used to find the flame speed. The camera was fixed in specified location and pictures were taken at a speed of 30 frames per second. The speed was found from these pictures.

To calculate flame speed from high speed camera: The time needed to travel 13.5 cm is 0.3462 second.

So the flame speed is calculated as; S_L = (0.135/0.3462 = 39 ms^{-1}).

To calculate FA, given Methane partial pressure P_M = 8.4 kPa, and air partial pressure P_A = 60 kPa, n_M and n_A are mole of methane and air, respectively.

$$\text{Then, FA} = \frac{n_M}{n_A} = \frac{P_M}{P_A} = \frac{8.4}{60} = 0.14$$

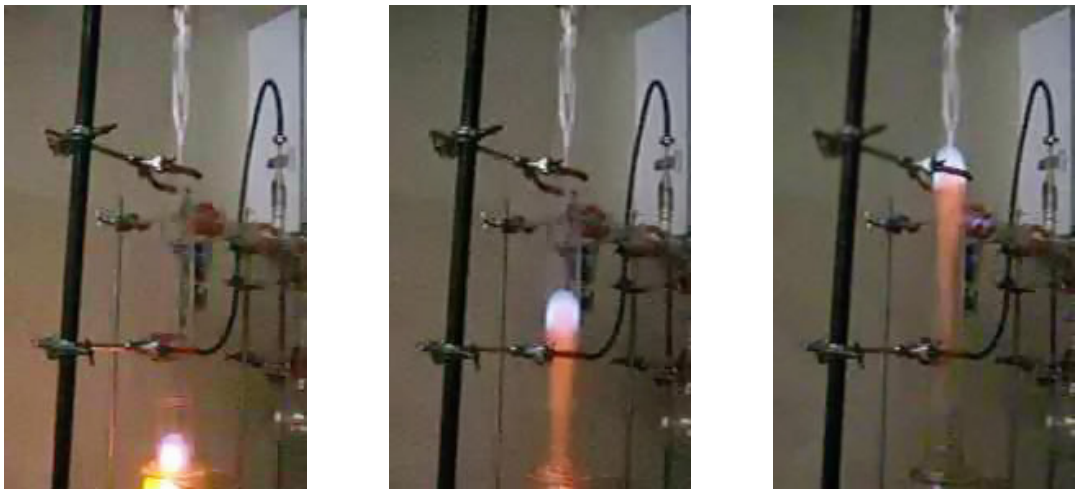

(frame 1) (frame 5) (frame 9)

Figure 3.7: Photo a flame when ignition was started (frame 1), after 0.1333 second (frame 5) and after 0.3535 second of first frame (frame 9)

Fig. 3.7 shows three flame potations during experiments (methane-air ratio is 14% and with no addition of CO_2).

Flame speed was measured by knowing the individual distance between each two photovoltaic cells and counting the time interval using the digital display on the computer as mentioned.

The whole distance is 0.405m, which was divided by four photovoltaic cells into three intervals of 0.135m for each cell, they was distributed on a column such as one at the bottom, and one each 0.135m.

3.2 Experimental Procedure

Flammability limits were determined for flame upwards propagation in a cylindrical ignition tube using apparatus in Fig. 3.1.

The gas mixtures of the needed compositions were prepared in a spherical mixing flask injected directly from the gas cylinders.

They were then allowed to mix by diffusion for a period of forty five to sixty minutes before being admitted to the vertical ignition tube.

Ignition was initiated by an electric spark at the bottom of the ignition tube. In some cases, a pilot flame was used to ignite some mixtures because of electric spark weakness. Four equally spaced photovoltaic cells assembly were used to measure the time needed by the flame front to reach certain level (depending on the inhibitor's effectiveness). They were located just in front of the ignition tubes. The four cells covered all the distance up to the end to capture any flame front reaching that level.

The time between each two series photovoltaic cell was measured using a PLC connected to a computer to display readings hence the flame velocity was measured. The flammability limit point was determined by trial and error technique until two very close mixture compositions were found. When one of mixtures propagated the whole length of the tube and the other did not the flammability limit was taken as the mean of these two compositions.

For each composition the apparatus was thoroughly evacuated down to less than 20 Pa. This was achieved by the use of rotary high vacuum pump. The gases (methane, air, nitrogen, carbon dioxide) were admitted to the apparatus as shown in Fig. 3.1. The connecting tubes to the apparatus were thoroughly flushed with each gas before use. The additive was introduced into the apparatus in a bulb in gaseous form at room temperature then added to the experimental mixtures.

During the experiments, it was necessary to introduce a small quantity of silicon layer to glass plate located at the bottom of combustion column and to the rubber stop at the top to prevent possible leakage to and from the closed combustion system.

3.3 Experimental Observations

In general, and during the experimental work it was noted that when approaching both the rich and lean flammability limits, ignition becomes progressively hard, while ignition becomes easier away from the two flammability limits.

Further, it was noticed that without the addition of an inhibitor to determine both rich and lean flammability limits of methane-air mixture, with reference to Fig. 3.8 and Fig. 3.9, blue flame front, propagates upwards with a rather low speed, this speed is reduced approaching the flammability limit.

Figure 3.8: Photo of methane-air flame at ignition point.

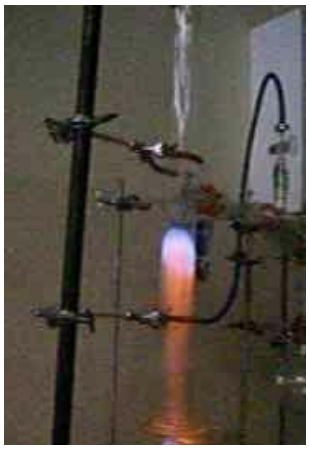

Figure 3.9: Photo of methane-air flame color without addition of inhibitors.

Greater amount of gases were evolved in finding rich flammability limit than the case of lean flammability one. Most of this gas evolved more in upward direction in the ignition tube, while the remaining amounts leave the tube through the opening at the bottom.

(1) CO_2 additive:

Using CO_2 as an inhibitor, the following were noted Fig. 3.10:

a) When a methane-air mixture is ignited an orange flame front was produced.

b) The flame was weak and reaches the upper part of ignition tube.

c) In the determination of the flammability limits, a thick luminous flame was observed when ignition occurs.

d) Because of the addition of carbon dioxide, a sharp smelling gas observed.

e) At a later stage of addition carbon dioxide the smell reduced to a certain level, but comparatively it was noted.

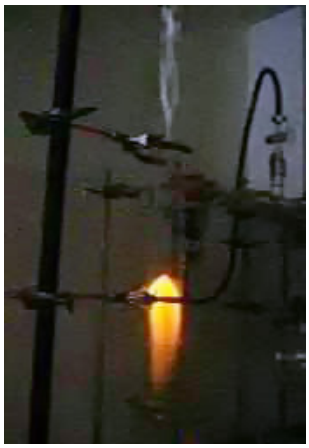

Figure 3.10: Photo of methane-air flame color with addition of CO_2.

f) It was observed that the continuation of carbon dioxide addition reduces the flame speed propagating in the ignition tube. The reduction was noted at higher percentage of carbon dioxide rates.

g) A full orange flame front was produced according to increasing amount of carbon dioxide in the combustible mixture. This color reached after a light orange flame front gradually tended to be strong orange one.

(2) N_2 additive:

Using N_2 as an inhibitor, the following were noted, see Fig. 3.11:

Frame (1)

Frame (2)

Frame (3)

Frame (4)

Frame (5)

Frame (6)

Frame (7)

Frame (8)

Frame (9)

Figure 3.11: Photo of frames from 1 – 9 present views for nitrogen inhibited methane air flame.

a) When the mixture is ignited a bluish flame front was produced but in higher tendency to blue color, flame front, than carbon dioxide one.

b) The speed of the flame is still higher, but it reduced as the flammability limits are approached, here, the reduction was gradually less than the carbon dioxide but it is still less than it when pure mixture is ignited.

c) In the flammability limits determination, thicker luminous flame observed when ignition occurs; this luminous was thick, compared to carbon dioxide flame.

d) As nitrogen gas is added, a sharper smelling gas was observed; this smell continued to be noted at higher rates of nitrogen addition.

e) At a later stage of nitrogen addition the gas smell was not reduced, it was noted at all levels of nitrogen addition, but comparatively it was less.

f) It was observed that the continuation of nitrogen addition reduces in small amounts the flame speed propagating in the ignition tube. The reduction was almost small between two steps of additive, but noted when comparing initial low and final high percentage of nitrogen rates.

g) A green bluish flame front was produced according to increasing amount of nitrogen in the ignition tube. This color reached after a bluish flame front gradually tended to be green bluish one.

3.4 Experimental Results

As have been already presented earlier, the flammability limits of the investigated mixtures were determined by the trial and error technique. This was done for each mixture in turn. The experiment (for a given inhibitor concentration) was

repeated several times and the flammability limits were taken as the average of the readings obtained.

The data shown below represents the variation of the upper and lower flammability limits for each inhibitor as a function of the inhibitor's concentration.

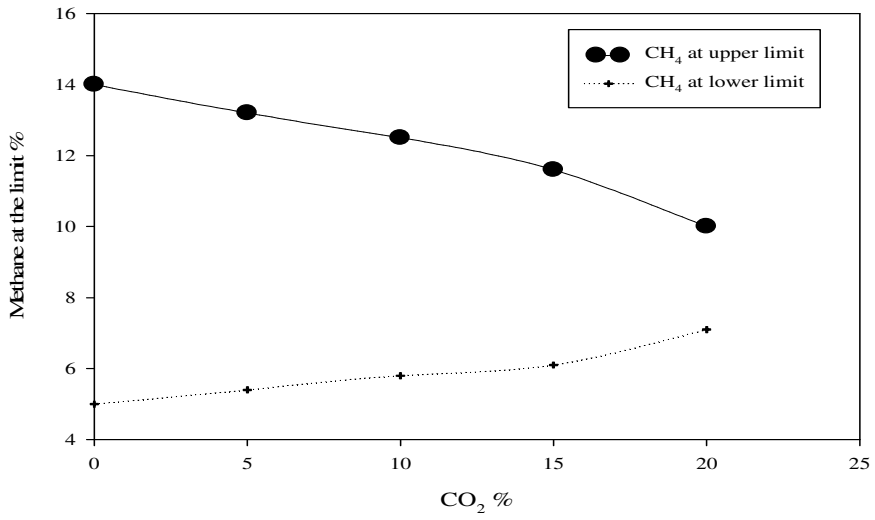

Figure 3.12 Methane-Air Rich and Lean Flammability limits as CO_2 Inhibitor used.

Referring to Fig. 3.12 and 3.13, it is noticed that the flammability limits are becoming narrower as the inhibitor's concentration is increased.

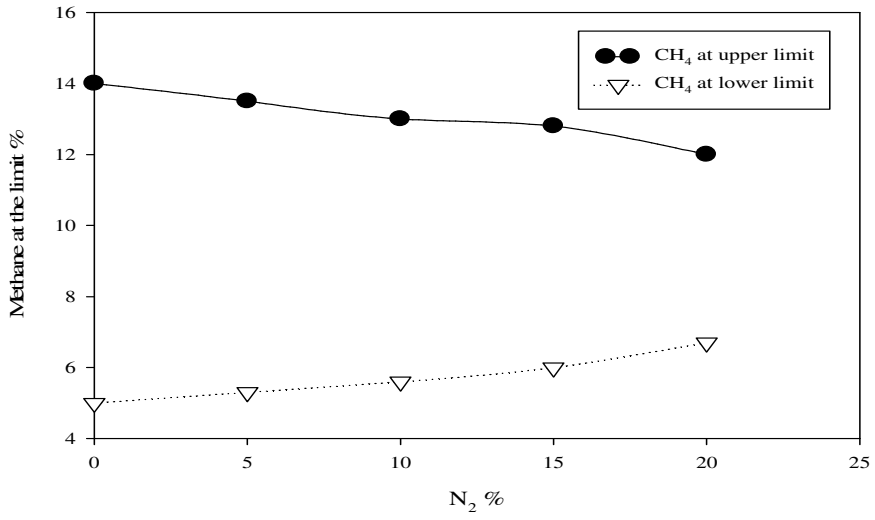

Figure 3.13 Methane-Air Rich and Lean Flammability limits as N_2 Inhibitor used.

The narrower limits are reached at the 20% inhibitor (i.e., 10.0 and 7.0 for upper and lower limit, respectively for CO_2 inhibitor and for N_2 inhibitor is varied between 12.0 and 6.7 for rich and lean limit, respectively), while the wider obviously seen at pure mixture 0% inhibitor (i.e., 14.0 and 5.0 for rich and lean limit, respectively).

At the upper limit the flame has maximum tendency to flash back in an ordinary burner and the combustion wave may develop into a detonation wave inducing an explosion hazard.

Hence upper explosion limit may be considered an index of explosion risk. The inhibitor used lowered this largely by reducing the concentration of free radicals in the flame boundary, increasing the difficulty of ignition, and thus increasing safety.

The narrower limit of nitrogen inhibitor is (12.0 to 6.7) is larger than that of carbon dioxide (10.0 to 7.1).

This indicates that CO_2 showed better inhibition effect on methane flame than N_2. Further, it is clearly seen from the figure that the rate of change (decrease) of the limits for CO_2 is greater than that for N_2.

This indicates that for a given inhibitor's concentration, the effect of CO_2 addition is greater than that for N_2.

Results presented in Fig. 3.14 and 3.15 show the variation of flame speed with percentages of inhibitors.

To help understand and interpret each figure, a brief illustration of the procedure followed to obtain the flame speed is shown below.

Flame speed was measured using four equally-spaced photo cells. By dividing the distance between each two photovoltaic cells to the time needed by the flame to cover this distance, we obtained the flame speed.

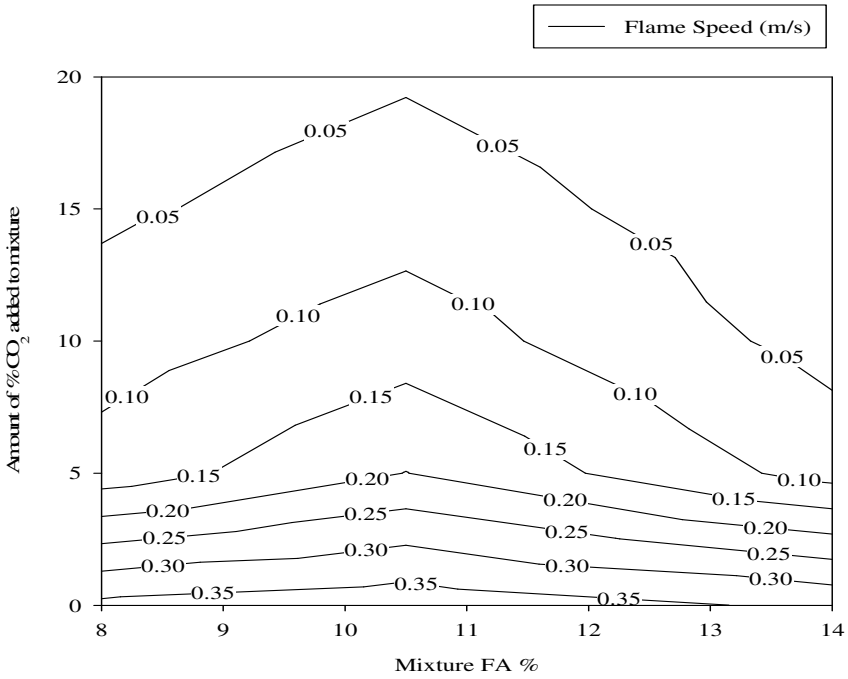

Figure 3.14: Flame speed at methane-air ratio = 8%, 10.5% and 14% while using different CO_2 quantities.

Fig. 3.14 shows the effects of CO_2 inhibitor on flame speed. The fuel-air ratios used were chosen as follows; one value near the lean limit 'FA ratio = 8 %', another one was taken at stoichiometric point 'FA ratio = 10.5%', and the last one was chosen near the upper limit 'FA ratio = 14%'.

It is noticed that near the stoichiometric ratio, the flame speed is maximum. Beyond this ratio the flame speed drops down.

With the addition of CO_2 it can be noticed that for all mixtures, the flame speed drops down. This is expected due to the inhibition effect of CO_2.

Figure 3.15 shows the same data as that of the previous one but with N_2 as inhibitor.

There is clear difference in the rate and amount of reduction in flame speed with inhibitor's concentration.

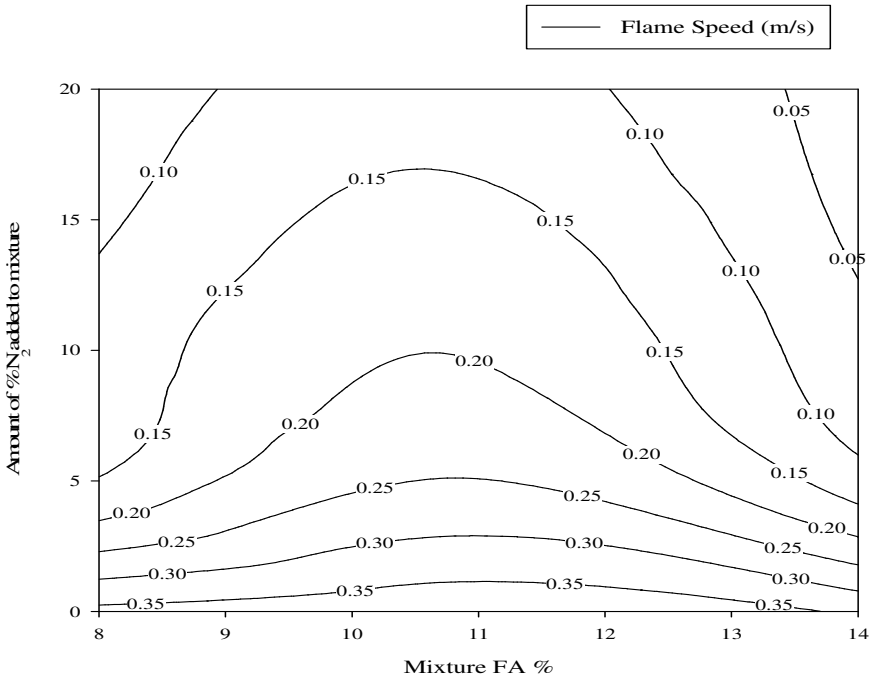

Figure 3.15: Flame speed at methane-air ratio = 8%, 10.5% and 14% while using different N_2 quantities.

This indicates that CO_2 has a stronger effect in reducing methane-air flame speed. Also, it is noticed that (within the range of inhibition studied) both gases has no appreciated inhibitory effect; because they must supplied in large quantities in order to inhibit or reduce speed for the methane air flame.

The above discussion is summarized in the following Tables 3.2 and 3.3 showing the results for flame speed (m/s), volume basis of fuel to air ratio, for both CO_2 and N_2 additives respectively.

One could find that the methane-air flame speed is reduced when carbon dioxide gas is added to a gaseous mixture and the reduction is continued while increasing amounts of inhibitor, in Table 3.2, this is obvious in the rich limit at FA 14% (flame speed reduced from 0.34 m/s to 0.00 m/s). But flame speed is increased according to the removal of inhibitor from the combustible mixture. This is obvious in the lean limit at FA 8% (flame speed increased from 0.019 m/s to 0.362 m/s).

Table 3.2 Methane-Air flame speeds as CO_2 inhibitor is used.

Percentage of CO_2 added % (v/v)	FA 8%	FA 10.5%	FA 14%
	Speed (m/s)	Speed (m/s)	Speed (m/s)
0	0.362	0.382	0.34
5	0.121	0.201	0.08
10	0.0753	0.126	0.032
15	0.041	0.077	0.15
20	0.019	0.045	0.00

On the other hand, following results are found when nitrogen inhibitor is used to reduce flame propagation by means of reducing its speed in vertical ignition tube.

In Table 3.3, speed (m/s), volume basis fuel to air of methane, and all of that data are collected with respect to N_2% additive.

Table 3.3 Methane-Air flame speeds as N_2 inhibitor is used.

Percentage of N_2 added % (v/v)	FA 8%	FA 10.5%	FA 14%
	Speed (m/s)	Speed (m/s)	Speed (m/s)
0	0.362	0.382	0.34
5	0.153	0.25	0.122
10	0.12	0.199	0.065
15	0.091	0.165	0.038
20	0.067	0.126	0.0262

It is found that the methane-air flame speed is decreased when nitrogen inhibitor is added to methane air gaseous mixture and the reduction is continued due to increasing amounts of inhibitor, in the upper part of Table 3.3, this is obvious in the rich limits from (14.0 to 10.0, for 0.0% N_2 and 20% N_2 additive, respectively).

Here, flame speed is increased according to the removal of inhibitor from the combustible mixture. This is obvious in the lean limit at FA 8% (flame speed increased from 0.067 m/s to 0.362 m/s).

Another evidence for carbon dioxide inhibitor efficiency, is that (at 20% inhibition ratio and 8% FA) the flame speed value of methane-air mixture is (0.067 m/s) for nitrogen and for carbon dioxide is (0.019 m/s) i.e., flame speed for N_2 is three and a half times that of CO_2.

Chapter Four

Discussion of Results

The simulation tool was necessary in spite of the presence of the experimental apparatus in order to investigate new inhibitors that could not be obtained in Jordan (e.g. Sulfur Dioxide) and also to have an inside look at the inhibitor's mechanism.

The model used for the simulation was the latest available up-to-date GRI-Mech with its thermodynamic and transport data files *(see A.4)* and *(see A.5)*.

At first, the theoretical model was verified with pure methane combustion. Since, GRI-Mech is made for the combustion of methane, the conditions prevailing at the experiment were fed to the model and the results (theoretical) were compared with those of the experiment.

Later, the model was modified with the inclusion of newly suggested equations depending on the inhibitor used (Appendices A.5, A.7, and A.8).

The results obtained were verified against the data obtained experimentally using all the inhibitors studied.

This step was of most importance in order to validate the mathematical model for further use.

4.1 Model Validation through Experimental and Theoretical Data

The model validation with the case of pure methane as well as carbon dioxide inhibitor is presented in Fig. 4.1 while Fig. 4.2 shows the same for nitrogen inhibitor, both under different AF ratios. Differences are obvious numerically, but they have same trends.

Curves show that at same inhibition rate the experimental slightly differs from the theoretical data, a 10.8% of error was found in Fig. 4.1 between experimental and theoretical values, for CO_2 inhibitor.

While in Fig. 4.2, average percentage of error of less than 8.5% is recorded for N_2 comparison.

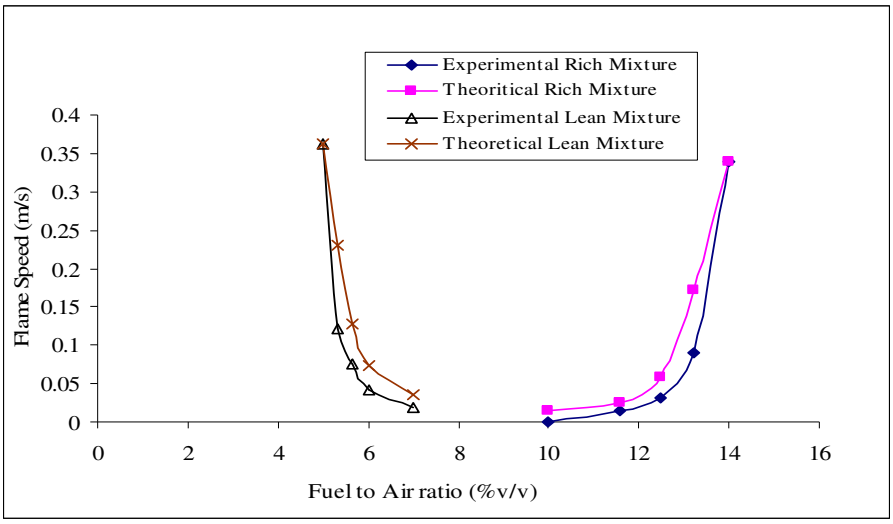

Figure 4.1: CH_4–Air flame model verification at different % of CO_2 (Velocity VS F/A ratio) curve.

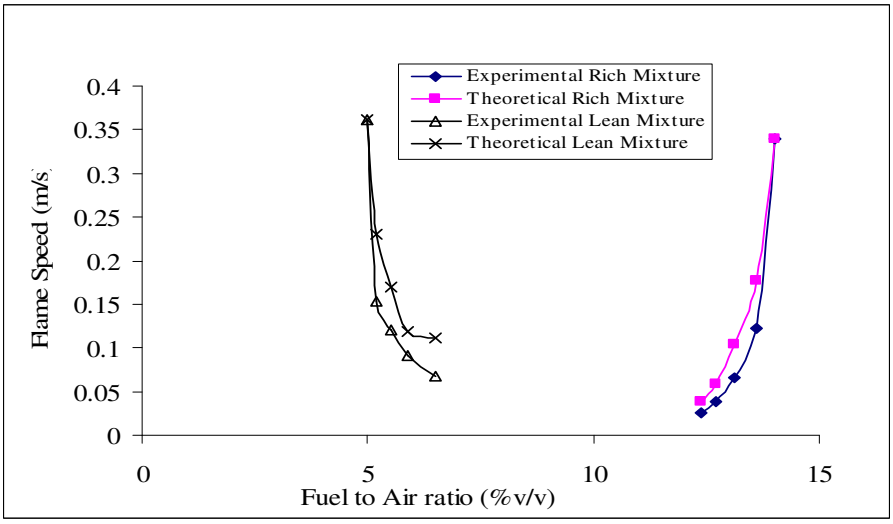

Figure 4.2: CH_4–Air flame model verification at different % of N_2 (Velocity VS F/A ratio) curve.

It was found that the flame speed at stoichiometric point without addition of any inhibitor is about 0.39 m/s while the same value was obtained experimentally to be 0.40 m/s.

According to the above, it is concluded that the model is now verified with the expected, and hence, further analysis can be carried out.

The next comparisons are made between the three inhibitors used in the study, CO_2, N_2, and SO_2.

Fig. 4.3 shows variation of flame speed with variable inhibition amounts of CO_2, N_2, and SO_2 and fixed equivalence ratio, lean mixture (8% F/A, v/v).

It is obvious that carbon dioxide has minimum slope trend and nitrogen has maximum trend, and sulfur dioxide has an intermediate at most of the curves drawn above.

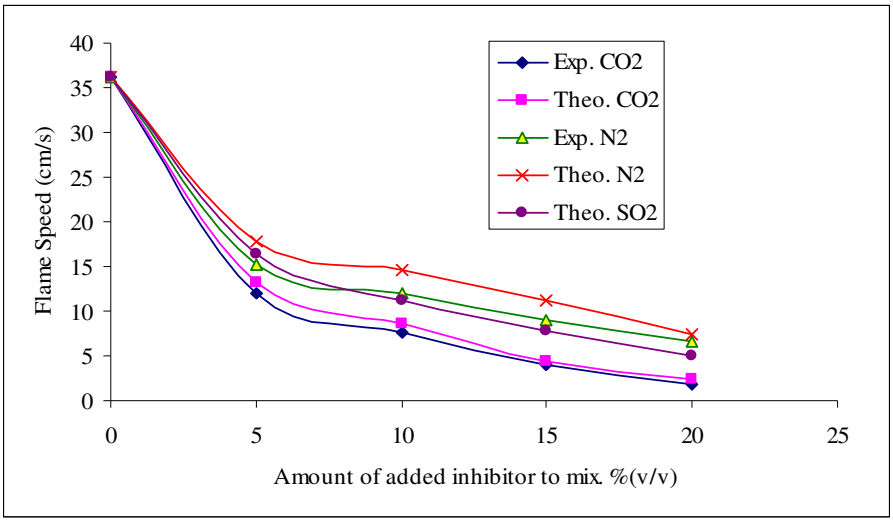

Figure 4.3: Flame speed at methane-air ratio (8%) while using different quantities of CO_2, N_2, and SO_2.

Fig. 4.4 shows similar plot to previous one, but at stoichiometric mixture (10.5% FA, v/v).

Same as before carbon dioxide has minimum slope trend and nitrogen has maximum one, sulfur dioxide is the intermediate one.

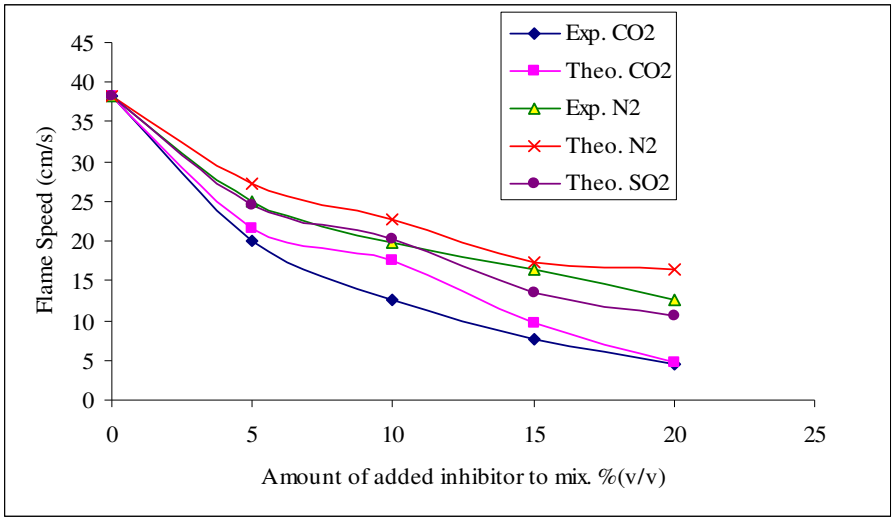

Figure 4.4: Flame speed at methane-air ratio (10.5%) while using different quantities of CO_2, N_2, and SO_2.

Next Fig. 4.5 shows similar to previous two plots, with rich mixture (14% FA, v/v).

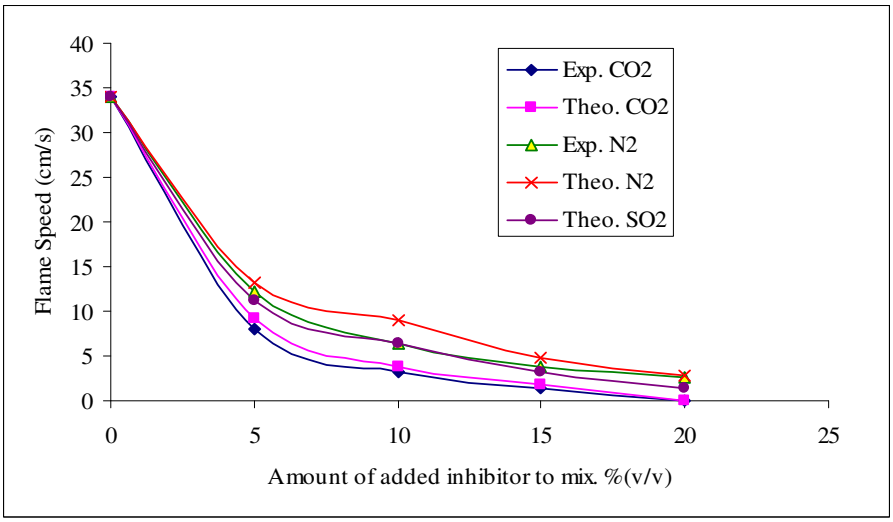

Figure 4.5: Flame speed at methane-air ratio (14%) while using different quantities of CO_2, N_2, and SO_2.

Again, carbon dioxide has minimum slope trend, next sulfur dioxide and, at last, nitrogen has maximum trend.

4.2 Distance, Velocity and Percentage of Inhibition Simulation

The following discussion is based on simulation data which resulted from the addition of different types of inhibitors to methane air flame mixture:

4.2.1 Addition of CO_2 *(see A.6)*

Fig. 4.6 shows the variation of flame speed along the path for carbon dioxide inhibitor. It is noted that increasing CO_2 percentage within 2-12% (v/v) has no effect on the flame speed since low velocity is registered.

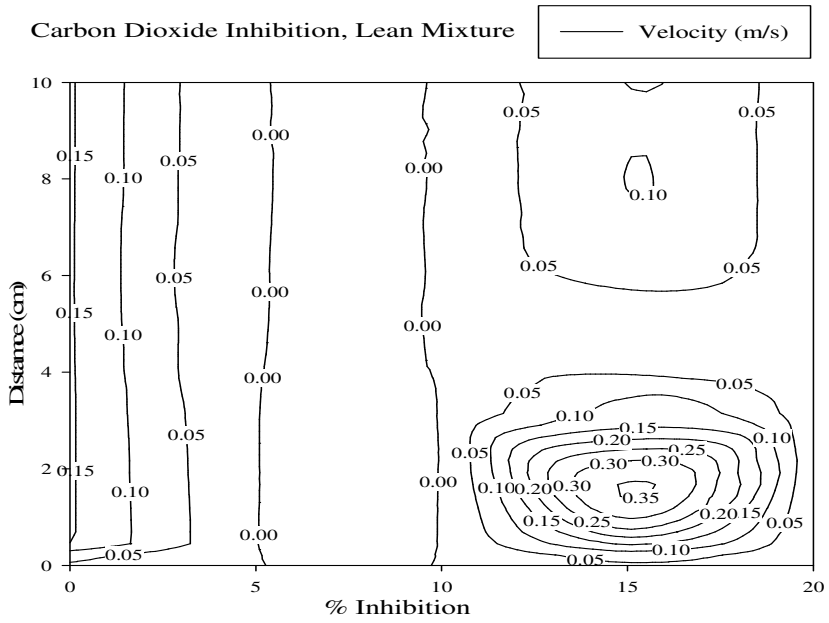

Figure 4.6 Simulated Inhibition of lean CH_4–Air flame with CO_2 inhibitor

However, at distance of 2cm along the ignition tube, increasing amounts of CO_2 from 12% to 19% makes velocity increases for a maximum point at 15% rate of inhibition (amount of added inhibitor) to a value of 0.35 m/s, and preserving velocity end values between 0.05 m/s at ends of high velocity region. This can be understood due to high temperatures and rates of dissociation that carbon monoxide CO radical

plays an important role at that region, especially in lean mixtures. Data presented here, show no effects for the CO radical.

However, this incremental velocity rise is related to high temperatures due to immediate ignition at the beginning of combustion process, which occurs at the beginning of ignition tube. Increasing inhibition rates for CO_2 provides a good chance for CO radical to continue the reaction in flame front region and sustain velocity of flame in lean mixture. Since there is no sufficient fuel to continue combustion process, CO radical completes the missed chain in that way, this is an important point, which might be summarized as not always increasing amounts of additives will reduce flame velocities and therefore extinguish fires. Fig. 4.7 represents rich mixture behavior due to ignition by use of CO_2 inhibitor, differently.

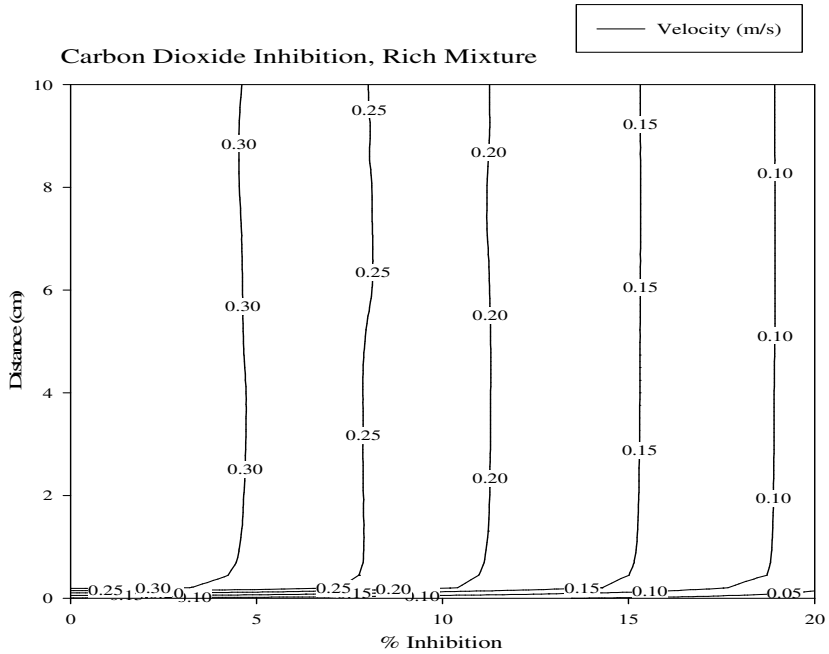

Figure 4.7 Simulated Inhibition of rich CH_4–Air flame with CO_2 inhibitor

The effect of addition of carbon dioxide is not clear at the beginning of combustion process and at small CO_2 inhibition rates, but at values from 5% to 20% rates of CO_2, the velocity drops from 0.3 to 0.1 m/s, respectively, along the ignition

tube. The case is not like lean mixture, since there is a sufficient amount of fuel which is ready to burn before and out of the ignition tube, this case makes inhibition with no effect at small rates on the rich mixture, but the efficiency of inhibitor dramatically increased with increasing amounts of inhibitor. Another observation can be made out of that figure, that is almost no change in velocity along the ignition tube itself at constant inhibition rate. This figure ends the incremental increase in CO_2 rates with a final velocity value of 0.2 m/s. Again, adversely compared to lean mixture, the rich mixture has differed behavior than that of lean. Since, as mentioned, there is no more than single velocity region in rich methane air mixture.

4.2.2 Addition of N_2 *(see A.7)*

When nitrogen inhibitor is used, results shown in Fig. 4.8 were plotted.

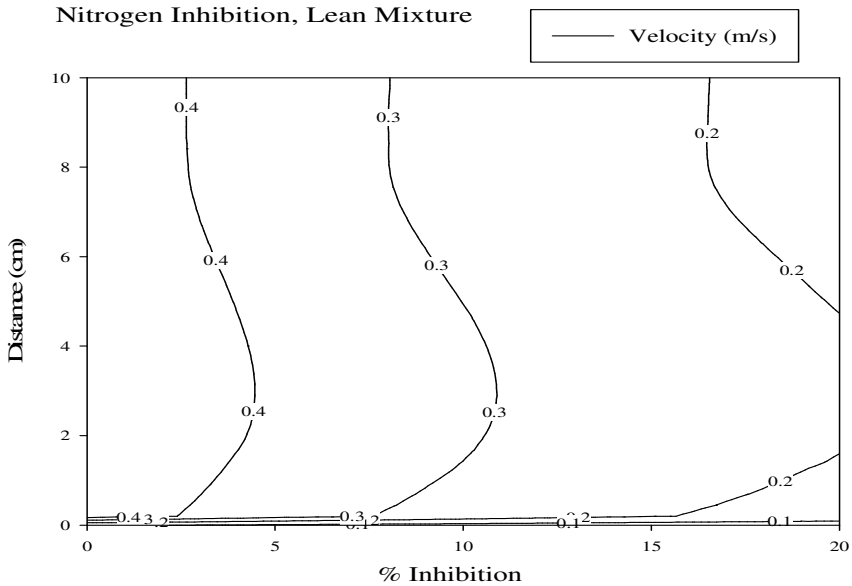

Figure 4.8 Simulated Inhibition of lean CH_4–Air flame with N_2 inhibitor

It is observed from that plot that increasing percentage of inhibitor has a slight effect on the flame speed which reduced from –almost 0.40 to 0.20 m/s- all over the nitrogen runs. At 2.5% of nitrogen additive the speed registered 0.4m/s, increasing

amounts of N_2 from 2.5% to 7.5% makes incremental decrease in velocity from 0.40 to 0.20 m/s, then an extra amount of N_2 reduces the flame speed to 0.1 m/s. At distances from 0.0 to 0.3 cm marked inhibition rates larger than rest of tube length, while that from 2.0 to 8.0 cm marked a slight inhibition rates. Data presented in Fig. 4.8, shows no effects of any radicals that might change flame speed, in large way, to moderate values. This is an important point which might be summarized as 'no evidences could initiate inhibition if there is o flame speed change, due to no excess variables of measurement'. Unlike CO_2, N_2 established no intermediate velocity regions, and therefore, effect of inhibition is still unfair compared with CO_2.

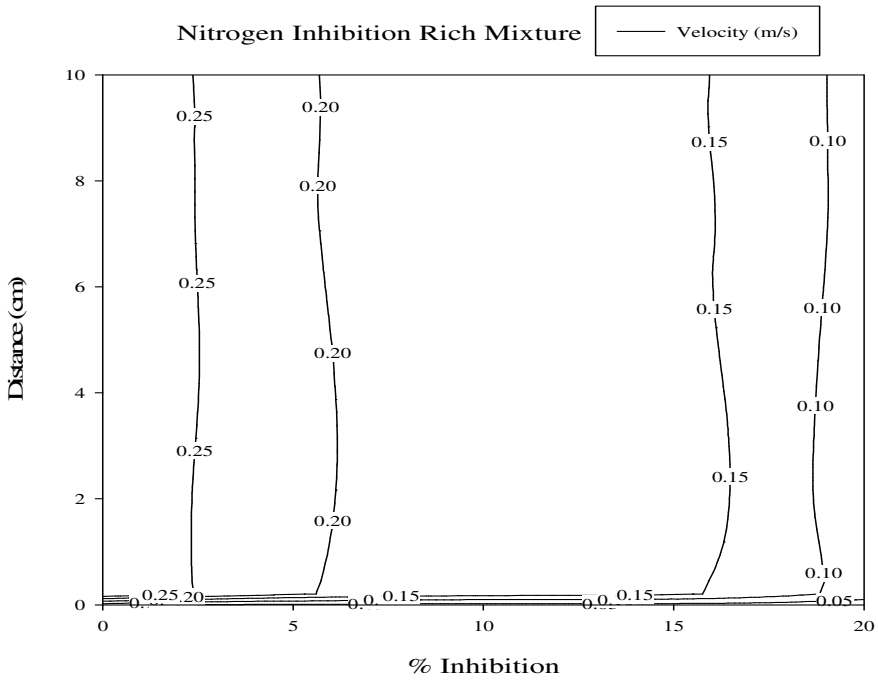

Figure 4.9 Simulated Inhibition of rich CH_4–Air flame with N_2 inhibitor

Fig. 4.9 represents a rich mixture behavior due to ignition by use of N_2 inhibitor, differently, the effect of addition of nitrogen is clear at the beginning of combustion process and at beginning of ignition tube, but at values from 2.5% to 17.5% rates of N_2, the velocity reduced from 0.25 to 0.10 m/s, respectively, along the ignition tube. The difference appeared from lean mixture, since there is sufficient amount of fuel, which is

ready to burn before, and outside the ignition tube. This case makes inhibition with no effect at small rates on the rich mixture, but efficiency of inhibitor dramatically appeared with increasing amounts of inhibitor. Another observation can be made is that there is no change in velocity along the ignition tube itself at constant inhibition rate. Again, like the lean mixture, the rich mixture has almost same behavior that lean has. Since, as mentioned, there is a stable velocity at constant inhibition rate. So, 'in nitrogen inhibition the rich and lean mixtures are agreed to have same velocity distribution among percentages of nitrogen additive'.

4.3 Comparison of Some Additives

Sulpher dioxide *(see A.8)* introduced to compare as an inhibitor with both nitrogen and carbon dioxide.

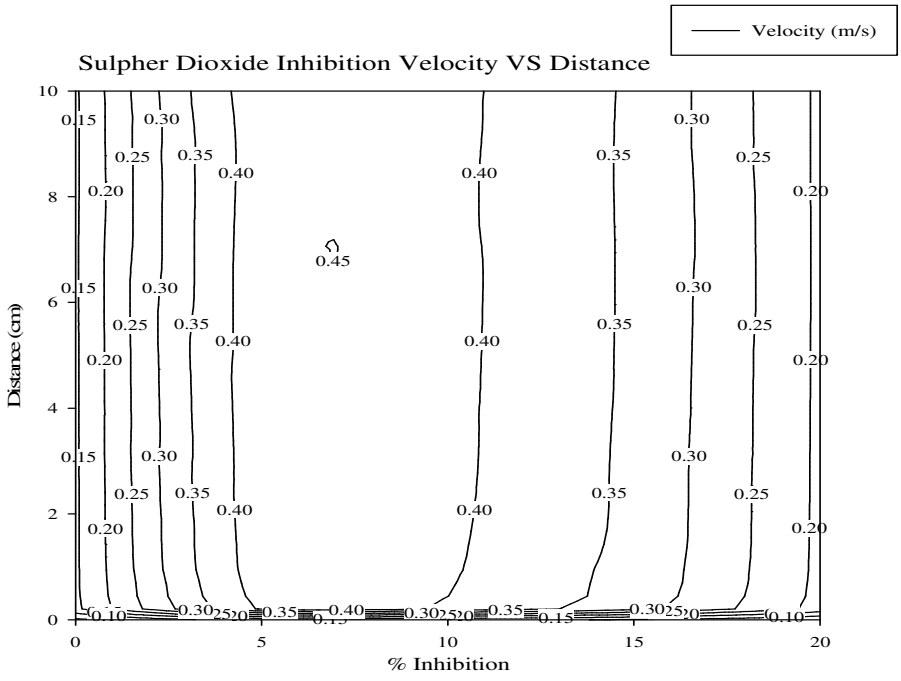

Figure 4.10 Simulated Inhibition of rich CH_4–Air flame with SO_2 inhibitor.

Initially Fig. 4.10 shows the behavior of sulpher dioxide in rich methane air mixture.

A rich content of methane air mixture result in high velocity flame propagation, and therefore, unstable inhibition characteristics occurs along increased percentages. Inhibition of flame occurs in low percentage levels in better way than that of intermediate levels, around 7.5% of SO_2 no effective retarding for flame velocity is noted, but at 2.5% and 17.5% of SO_2 the inhibition is better.

Next, in Fig. 4.11 the behavior of sulpher dioxide in lean methane air mixture presented. Inhibition of flame occurs in low percentage levels is more efficient than that of other levels, from (0 – 5) % of SO_2 an effective retarding for flame velocity is happened, and between (6 - 7.5) % of SO_2 the inhibition is stable along the ignition tube, except at the start end at the bottom.

At the far % of SO_2 there are no extreme differences that can affect the inhibition criteria. Stable characteristics of the lean mixture are dominant.

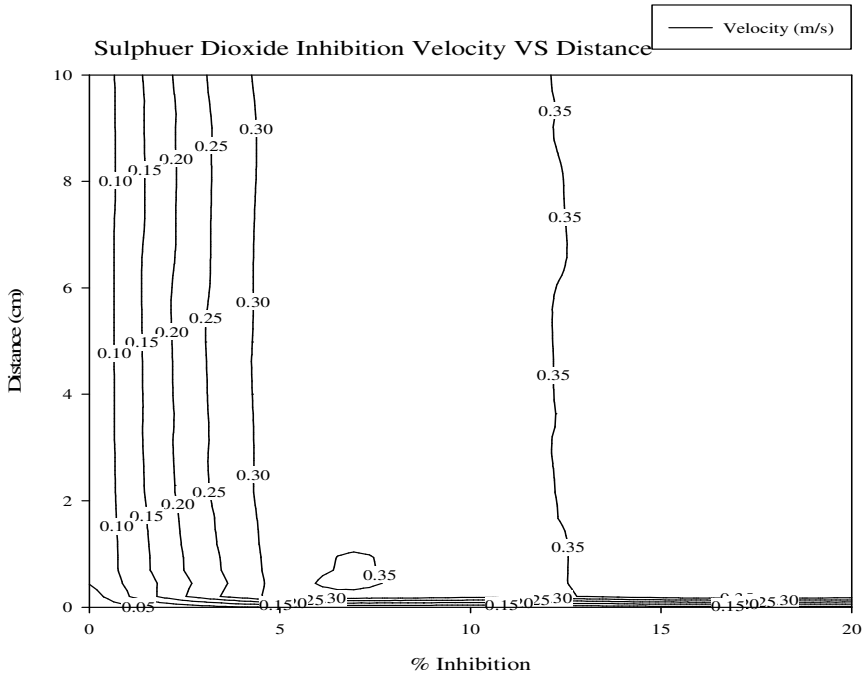

Figure 4.11 Simulated Inhibition of lean CH_4–Air flame with SO_2 inhibitor.

This was not the case of rich methane air mixture curve.

The two cases discussed later, emphasized on low flame velocities achieved for lean methane air flame mixtures compared to rich mixtures, when sulpher dioxide used as an inhibitor. Also in sulpher dioxide inhibition, the rich and lean mixtures agreed to have same velocity distribution among percentages of nitrogen additive. But there was a small difference in velocity profile for lean mixture.

Now, the case of comparison between the three inhibitors used in our study is presented in Fig. 4.12 through Fig. 4.14. In Fig. 4.12, comparison between CO_2 behavior in rich and in lean mixtures, burning velocity reduced from 0.36 m/s in its maximum to less than 0.019 m/s for lean mixtures, and for rich mixtures low flame velocity levels ranging between 0.34 and 0.0 m/s.

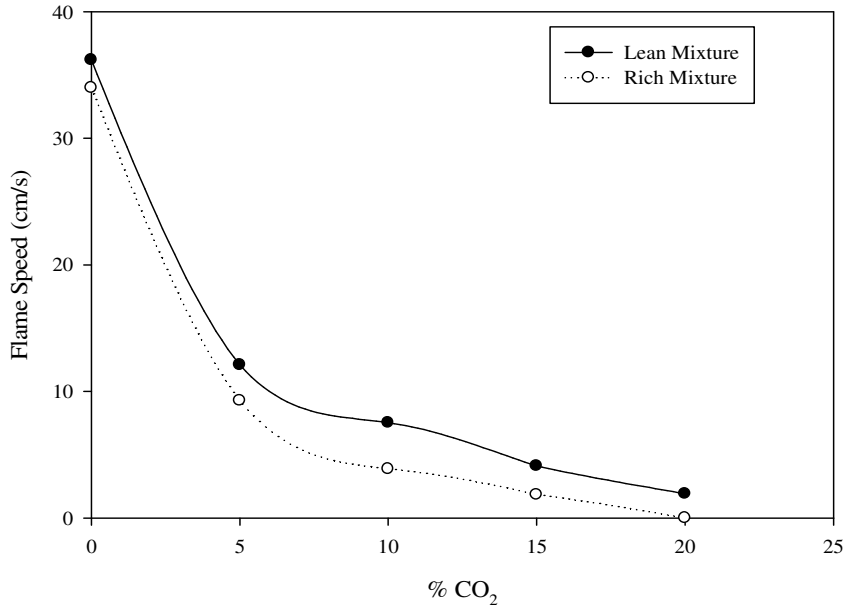

Figure 4.12 Simulated Inhibition of rich and lean CH_4–Air flame with CO_2 inhibitor.

Other comparison between N_2 behavior in rich and in lean mixtures found in next plot, Fig. 4.13 shows velocity levels for flames, velocity reduced from 0.36 m/s in its maximum to less than 0.073 m/s for lean mixtures, and for rich mixtures another velocity levels ranging between 0.34 m/s and 0.027 m/s.

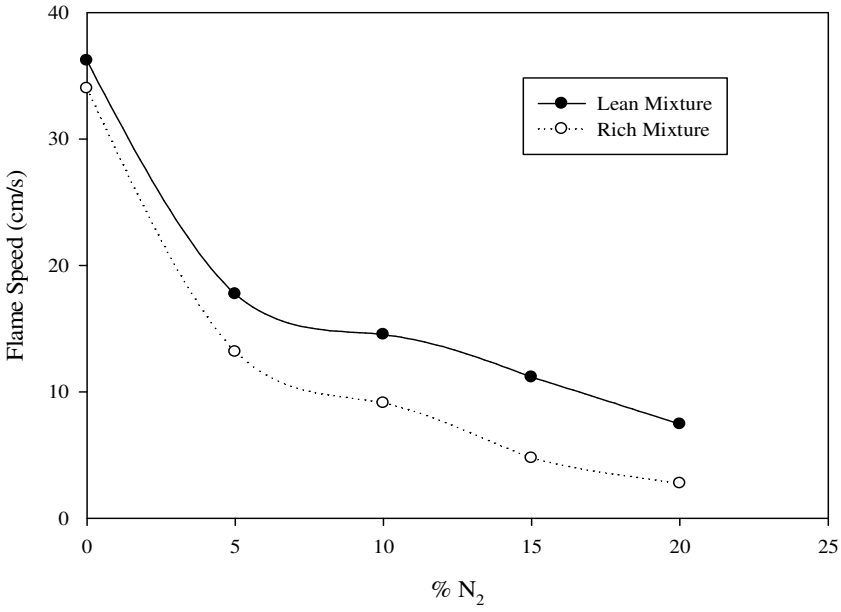

Figure 4.13 Simulated Inhibition of rich and lean CH_4–Air flame with N_2 inhibitor.

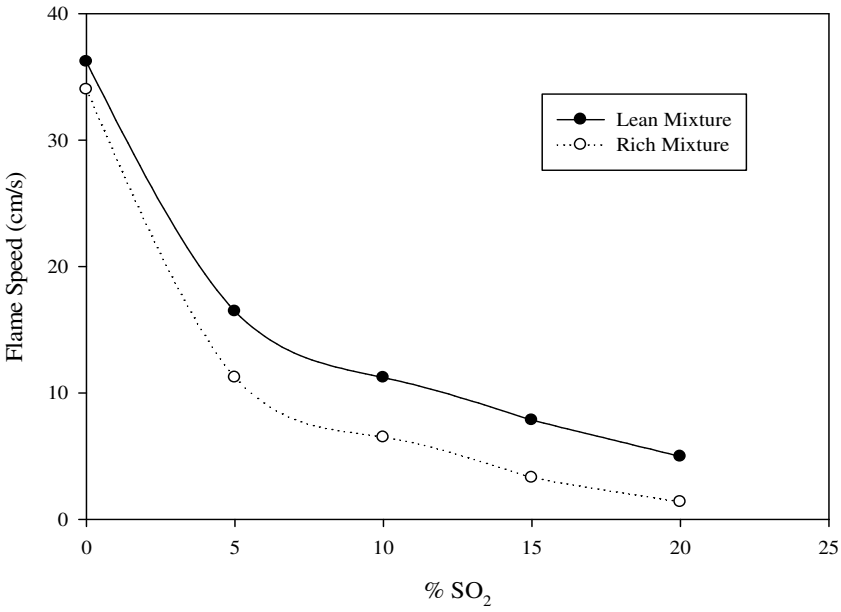

Figure 4.14 Simulated Inhibition of rich and lean CH_4–Air flame with SO_2 inhibitor.

Third comparison between SO_2 behavior in rich and in lean mixtures is presented in last plot, Fig. 4.14 gives a plot for maximum and minimum velocities in both rich and lean mixtures. For rich mixture, highest velocity of 0.34 m/s is occurred, and lowest velocity is 0.014 m/s, while for lean mixture highest velocity counted at 0.36

m/s and the lowest one at 0.049 m/s. From the above comparisons, numbers show that extreme lowest values of velocity was when carbon dioxide is used to distinguish the methane air flame in rich and lean mixtures, and extreme highest velocity was when nitrogen is used to inhibit the flame in lean mixture.

Other comparisons leads to same results and further discussion of chemistry plots will end in similar conclusions. This study gives an idea about the behavior of sulpher dioxide as inhibitor compared to known inhibitors nitrogen and carbon dioxide

4.4 Chemical Kinetics Comparison

In this section, a brief comparison of radical mole fraction is made for methane air mixture at constant percentage of inhibition (20% of each of the three inhibitors) and constant Φ (=0.65).

Fig. 4.15 shows the effect of H radical mole fraction consumption as CO_2, SO_2, and N_2 inhibitors used.

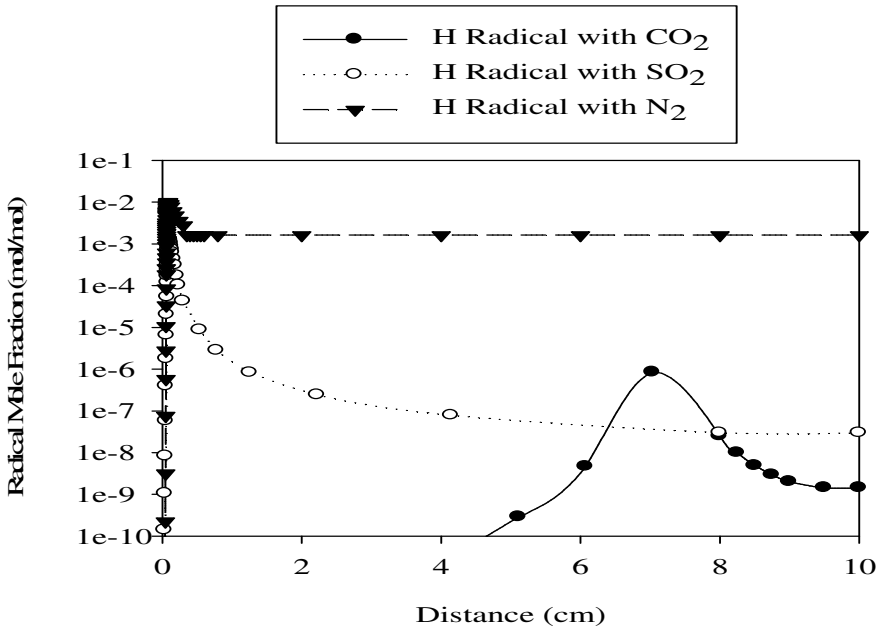

Figure 4.15 Simulated 20% (CO_2, SO_2, and N_2) Additive H-Radical to Methane-Air flame at Φ = 0.65.

Too small amounts of radicals are registered, and they consumed in retarding the flame speed.

The existing figure gives values of almost (1e-9 H radical) for CO_2 and (1e-7 H radical) SO_2 inhibitor at tube end, but (0.001 H radical) for N_2 inhibitor.

In Fig. 4.16 the effect of O radical mole fraction consumption as CO_2, SO_2, and N_2 inhibitors used is shown.

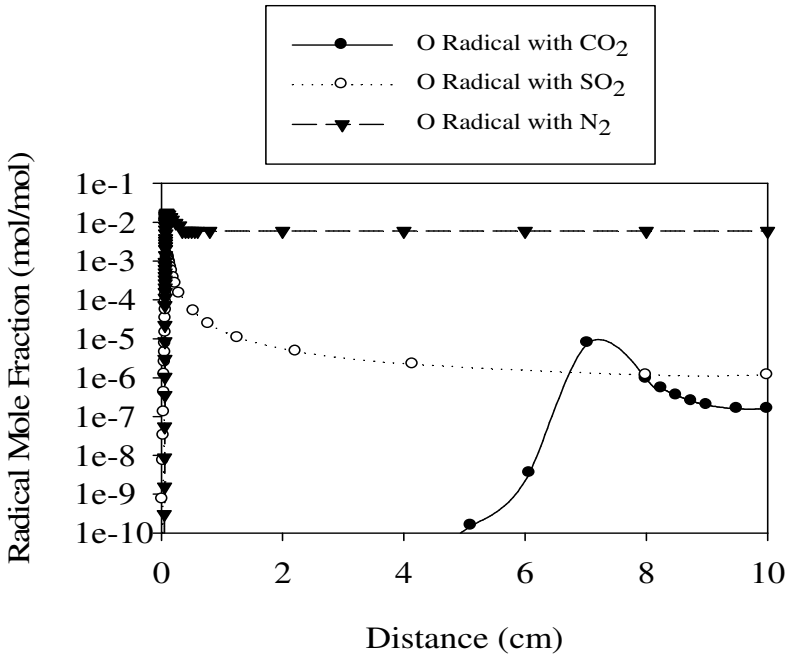

Figure 4.16 Simulated 20% (CO_2, SO_2, and N_2) Additive O-Radical to Methane-Air flame at $\Phi = 0.65$.

Also very small amounts of radicals observed, and they consumed in retarding the flame speed.

Fig. 4.16 presents values of almost (1e-6 O radical) for CO_2 and (1e-5 O radical) SO_2 inhibitor at tube end, but (0.001 O radical) for N_2 inhibitor.

Fig. 4.17 shows the effect of OH radical mole fraction consumption as CO_2, SO_2, and N_2 inhibitors used. Too small amounts of radicals are registered, and they consumed in retarding the flame speed. The existing figure gives values of almost (1e-5

OH radical) for CO_2 and (1e-4 OH radical) SO_2 inhibitor at tube end, but (0.015 OH radical) for N_2 inhibitor.

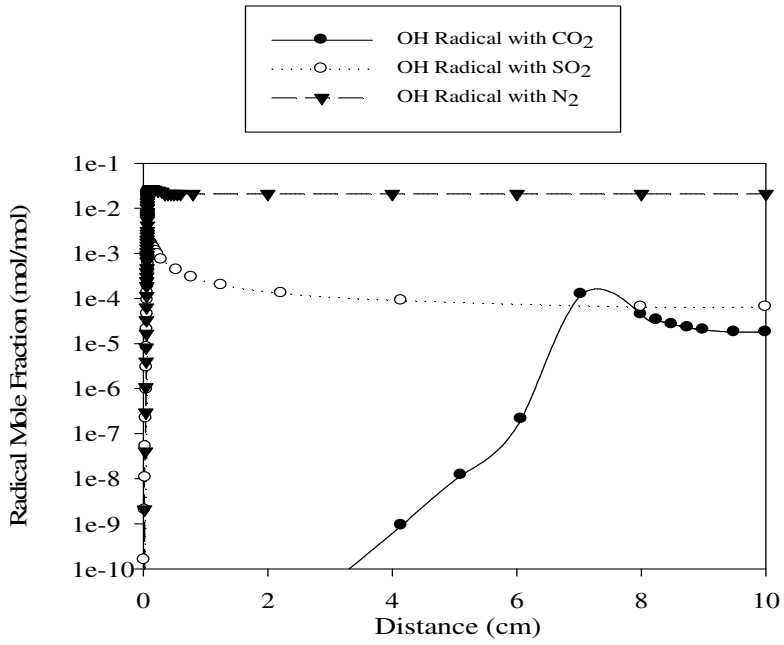

Figure 4.17 Simulated 20% (CO_2, SO_2, and N_2) Additive OH-Radical to Methane-Air flame at Φ=0.65

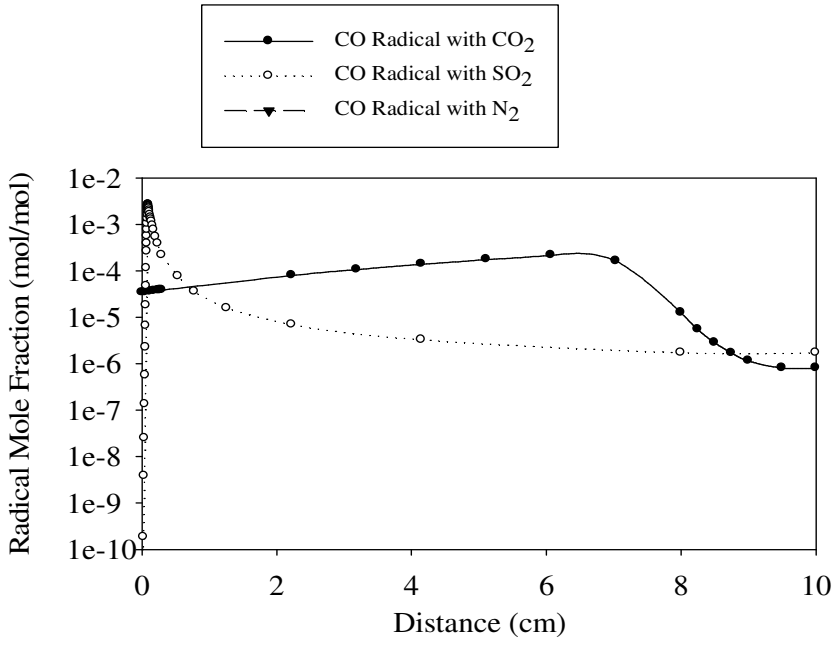

Figure 4.18 Simulated 20% (CO_2, SO_2, and N_2) Additive CO-Radical to Methane-Air flame at Φ=0.65

In Fig. 4.18 the effect of CO radical mole fraction consumption as CO_2, SO_2, and N_2 inhibitors used is shown. Also very small amounts of radicals observed, and they consumed in retarding the flame speed. The existing figure gives values of almost (1e-5 CO radical) for CO_2 and SO_2 inhibitors at tube end, but (0.001 O radical) for N_2 inhibitor. Fig. 4.19 shows the effect of CH_3 radical mole fraction consumption as in CH_4-air flame.

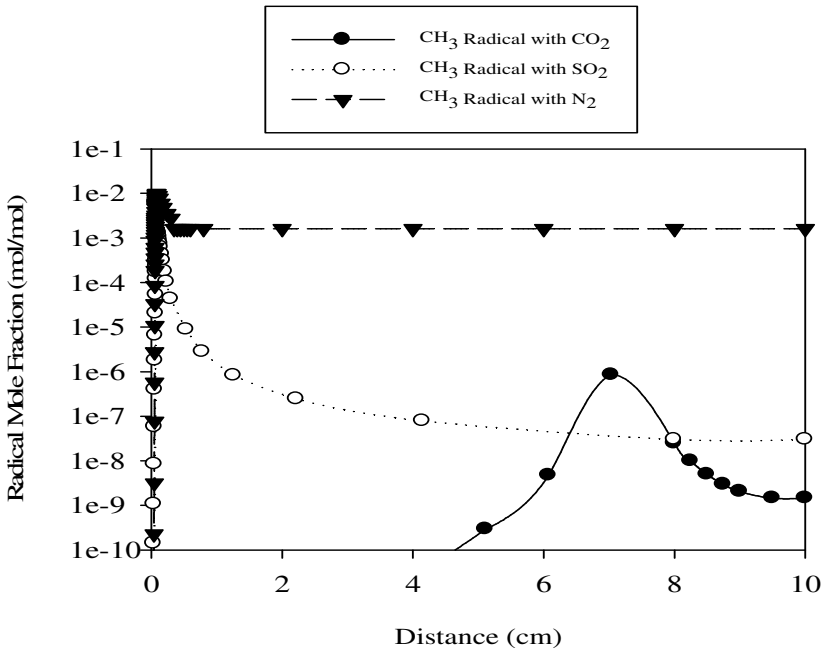

Figure 4.19 Simulated 20% (CO_2, SO_2, and N_2) Additive CH_3-Radical to Methane-Air flame at Φ=0.65

Definitely, no radicals in when CO_2 inhibitor is used. But little amounts of radicals are registered for SO_2 and N_2, and they consumed in retarding the flame speed. The existing figure gives values of almost (1e-5 CH_3 radical) for N_2 and (1e-7 CH_3 radical) for SO_2 inhibitor at tube start, but (zero CH_3 radical) for SO_2 inhibitor at rest of tube.

Too small amounts of radicals are registered, and they consumed in retarding the flame speed.

Fig. 4.20 provides values of almost (1e-5 CH_2 radical) for CO_2 and (1e-4 CH_2 radical) SO_2 inhibitor at tube end, but (0.1 CH_2 radical) for N_2 inhibitor.

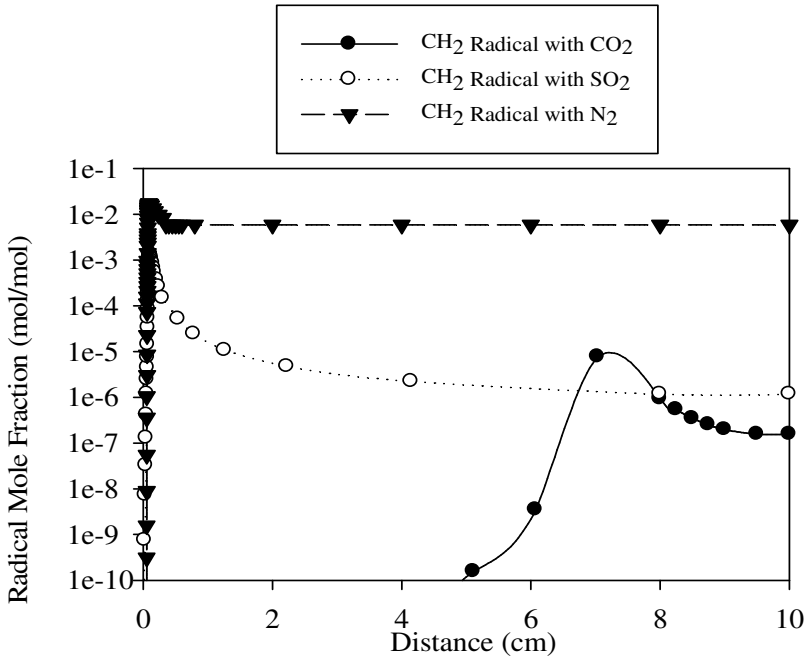

Figure 4.20 Simulated 20% (CO_2, SO_2, and N_2) Additive CH_2-Radical to Methane-Air flame at Φ=0.65

In Fig. 4.21 values are of almost (1e-5 CH radical) for CO_2 and (1e-4 CH radical) SO_2 inhibitor at tube end, but (0.1 CH radical) for N_2 inhibitor.

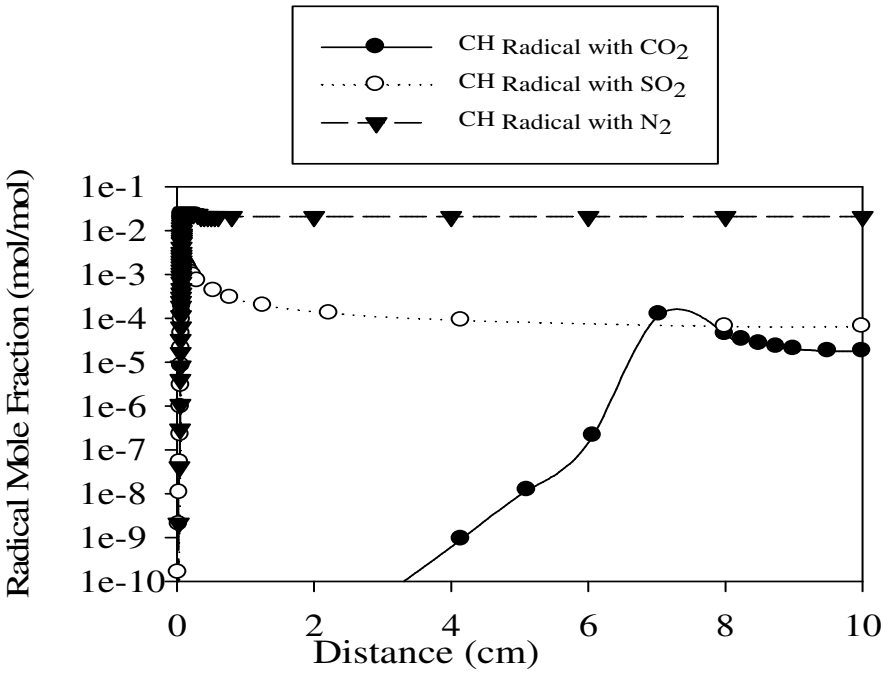

Figure 4.21 Simulated 20% (CO_2, SO_2, and N_2) Additive CH-Radical to Methane-Air flame at Φ=0.65

In Fig. 4.22 values are of almost (1e-6 CH_2O radical) for CO_2 and (1e-5 CH_2O radical) SO_2 inhibitor at tube end, but (0.01 CH_2O radical) for N_2 inhibitor.

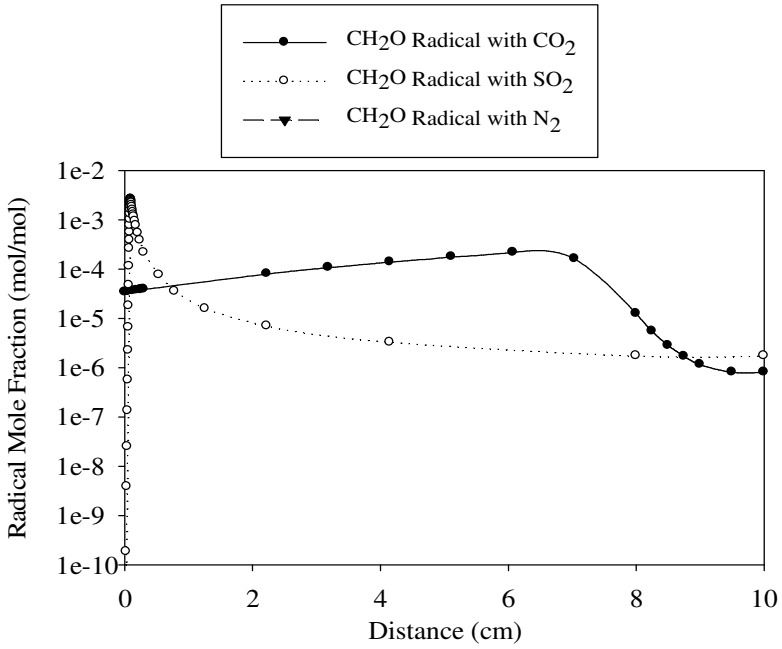

Figure 4.22 Simulated 20% (CO_2, SO_2, and N_2) Additive CH_2O-Radical to Methane-Air flame at Φ=0.65

From above compared numbers and figures, the existing of radicals is an evidence for flame continuation. It can be summarized, as shown in the table 4.1; all numbers are of low order of magnitude.

Table 4.1 Comparison between moles consumption for radicals at Φ=0.65 and 20% inhibition percentage.

Consumption / Radical	H	O	OH	CO	CH_3	CH_2	CH	CH_2O
With CO_2 inhibitor (1*e-)	9	6	5	5	1	6	5	6
With SO_2 inhibitor (1*e-)	7	5	4	5	7	5	4	5
With N_2 inhibitor (1*e-)	2	2	2	2	4	2	1	2

Therefore, the main reason of velocity retarding is ending of radicals and thus no more flame with high speed is need to be retarded. Selected radicals -*(see A.9)*- above were chosen from many radicals affecting the chain reactions of methane intermediate reactions.

4.5 Uncertainty Analysis

Refer to values given in pages 33 and 34, and by determination of individual uncertainty components using uncertainty law, experimental uncertainty for each measured variable could be summarized as follows:

* Time uncertainty using photovoltaic cells is obtained as

$\omega_{t1} = \pm 0.5 ms.$

This number is supplies with the sensor from the manufacturer.

* Time uncertainty using a digital camera is obtained as

$\omega_{t2} = \pm 16.67 ms.$

This number is supplies with the camera from the manufacturer.

* Distance uncertainty using a distance scale is obtained as

$\omega_{d} = \pm 0.5 * 1 mm = \pm 0.5 mm.$

This number half of the scale minimum reading.

* Flame speed uncertainty using a photovoltaic cell is obtained as,

$S_1 = 0.382$ m/s which is flame speed calculated from photovoltaic cell,

$$\frac{\omega_{s1}}{S_1} = \pm\sqrt{\left(\frac{\omega_d}{d}\right)^2 + \left(\frac{\omega_{t1}}{t}\right)^2}$$

$$\frac{\omega_{s1}}{S_1} = \pm\sqrt{\left(\frac{0.5}{135}\right)^2 + \left(\frac{0.5}{353.5}\right)^2} = \pm 3.9645 * 10^{-3}$$

$$\omega_{s1} = \pm 3.9645 * 10^{-3} * 0.382 = \pm 1.5144 * 10^{-3}$$

* Flame speed uncertainty using a digital camera is obtained as

$S_2 = 0.390$ m/s which is flame speed calculated from high speed camera,

$$\frac{\omega_{s2}}{S_2} = \pm\sqrt{\left(\frac{\omega_d}{d}\right)^2 + \left(\frac{\omega_{t2}}{t}\right)^2}$$

$$\frac{\omega_{s2}}{S_2} = \pm\sqrt{\left(\frac{0.5}{135}\right)^2 + \left(\frac{16.67}{346.2}\right)^2} = \pm 3.704$$

$$\omega_{s2} = \pm 3.704 * 0.390 = 1.5144 * 10^{-3} = \pm 1.444$$

* Fuel to air ratio uncertainty -for FA=14%- is obtained as

$$FA = \frac{n_M}{n_A} = \frac{P_M}{P_A}$$

where n_M= moles of Methane, and n_A= moles of Air

P_M= partial pressure of Methane, and P_A= partial pressure of Air

Knowing that $\omega_{P_A} = \pm 5(kpa)$, $\omega_{P_M} = \pm 1(kpa)$

$$\frac{\omega_{FA}}{FA} = \pm\sqrt{\left(\frac{\omega_{P_M}}{P_M}\right)^2 + \left(\frac{\omega_{P_A}}{P_A}\right)^2}$$

$$\frac{\omega_{FA}}{FA} = \pm\sqrt{\left(\frac{1}{8.4}\right)^2 + \left(\frac{5}{60}\right)^2} = \pm 0.1453$$

$$\omega_{FA} = \pm 0.1453 * 0.14 = \pm 0.0203$$

* Fuel to air ratio uncertainty –with FA = 8%, 10.5% and 14% for CO_2 and N_2 – can be obtained as

$$FA = \frac{n_M + n_{CO_2}}{n_A} = \frac{P_M + P_{CO_2}}{P_A}$$

for CO_2 additives. where n_{CO_2} = moles of CO_2,

$$FA = \frac{n_M + n_{N_2}}{n_A} = \frac{P_M + P_{N_2}}{P_A}$$

for N_2 additives. where n_{N_2} = moles of N_2,

P_{CO_2} = partial pressure of CO_2, and P_{N_2} = partial pressure of N_2

With $\omega_{P_A} = \pm 5(kpa)$, $\omega_{P_M} = \pm 1(kpa)$, $\omega_{PCO_2} = \pm 0.1(kpa)$,

and $\omega_{PN_2} = \pm 0.1(kpa)$

$$\frac{\omega_{FA}}{FA} = \pm\sqrt{\left(\frac{1}{7.98}\right)^2 + \left(\frac{5}{60}\right)^2 + \left(\frac{0.1}{0.42}\right)^2} = \pm 0.28167$$

$$\omega_{FA} = \pm 0.28167 * 0.14 = \pm 0.039433$$

Tabulated results for all data used are summarized in 4.2 below.

Table 4.2 Uncertainty analysis for all experimental F/A ratios

FA	0% (CO_2/N_2) ω_{FA}	5% (CO_2/N_2) ω_{FA}	10% (CO_2/N_2) ω_{FA}	15% (CO_2/N_2) ω_{FA}	20% (CO_2/N_2) ω_{FA}
14%	0.0203	0.039433	0.02751	0.02537	0.02528
10.5%	0.01883	0.03867	0.02640	0.024176	0.02408
8%	0.01795	0.038253	0.02579	0.02350	0.02340

From the above, it is shown that highest uncertainty value is 0.039433 and lowest value is 0.01795, the average uncertainty value for each FA ratio is 0.0275758 for (FA =14%), 0.026431 for (FA= 10.5%), and 0.025778 for (FA= 8%).

So the experimental average error did not exceed uncertainty value of 0.0275758 as an average.

Conclusions and Summary

A study of methane-air flame inhibition using three different inhibitors, named carbon dioxide, nitrogen and sulpher dioxide gases was performed. The percentage of inhibitors was varied in following rates 0, 5, 10, 15, and 20%. The combustion of the mixtures was carried out at atmospheric conditions. Following is a summery of the results found in this work:

a. The flame speed for pure methane-air combustion in upward propagation was nearly 40cm/s, and it decreased with presence of inhibitors.

b. For pure methane-air flame, the lower flammability limit (LFL) was found to be 5.0% and the upper flammability limit (UFL) was 14.0%.

c. When CO_2 was used as an inhibitor in (5, 10, 15, and 20%) the LFL's were (5.4, 5.8, 6.1, and 7.1%) respectively, and the UFL's were (13.2, 12.5, 11.6, and 10.0%) respectively.

d. Using N_2 in same percentages, the LFL's were (5.3, 5.6, 6.0, and 6.7%) respectively, and the UFL's were (13.5, 13.0, 12.8, and 12.0%) respectively.

e. The GRI-Mech model was used and modified to simulate the combustion of process. The modified model was successfully verified against experimental data.

f. Simulation of flame speed was made resulting in same trend for inhibition curves (Flame speed vs. FA ratio) compared to experimental curves.

g. Curves showed verification of simulated model against experimental data. The SO_2 inhibitor was simulated only with no experimental work because of its unavailability.

h. It was noted that (within the range and type of inhibitors used), an increase of inhibition ratio does not always have positive effect on the inhibition process.

i. SO_2 has better inhibition effect than nitrogen, however, it is less effective compared with carbon dioxide.

j. Among the inhibitors used and within the range of percentages studied, carbon dioxide showed best inhibitory characteristics, while nitrogen showed the least.

k. In nitrogen inhibition the rich and lean mixtures are agreed to have same velocity distribution among percentages of nitrogen additive.

l. In sulpher dioxide inhibition the rich and lean mixtures are agreed to have same velocity distribution among percentages of nitrogen additive. But there was a small difference in velocity profile for lean mixture.

m. Using burning velocity to measure inhibition of any chemical is a traditional idea, but there must be other parameters can be measured like emission gases which give an estimation of products that are resulted from the inhibition process.

n. Chemical kinetics comparison gives an indication to what is happening for flame velocity, how it could be affected by radicals found in the combustion process, and the effect of radical mole fraction on retarding flames.

o. Future work is recommended to investigate other inhibitors that can serve as fire retardants.

p. This work also points out the need for further studies on gas phase inhibitors and there thermodynamic and transport properties, which can be used in modeling and simulating required chemical kinetic processes.

References

1. F. J. W. Jacobus, Metal Catalysed Intumescence of Ployhydroxil Compounds, **PhD Thesis, University of Pretoria, South Africa** (2003).

2. V. Babushok, W. Tsang, Inhibitor Rankings for Alkane Combustion, **Combustion and Flames**, 123 (2000), pp 488-506.

3. Stephen R. Turns, **An Introduction to Combustion - Concepts and Applications**, 2nd ed. McGraw Hill Companies Inc, (2000).

4. M. F. M. Nogueira and E. M. Fisher, Effects of dimethyl methylphosphonate on a premixed methane flame, **Combustion and Flames**, 132 (2003), pp.352-363.

5. V. I. Babushok, K. L. Mcnesby, A.W. Miziolek, and R. R. Skaggs. Modeling of synergistic effects in flame inhibition by 2-H heptafluropropane blended with sodium bicarbonate, **Combustion and Flames**, 133 (2003), pp. 201-205.

6. Gregory T. Linters, Vadim D. Knyazev and Valeri I. Babushok, Inhibition of premixed methane flames by manganese and in compounds, **Combustion and Flames**, 129 (2002), pp.221-238.

7. M. A. Macdonald, T. M. Jayaweera, E. M. Fisher, and F. C. Gouldin, Inhibition of nonpremixed flames by phosphorus containing compounds, **Combustion and Flames**, 116 (1999), pp. 166-176.

8. V. Babushok, W. Tsang, G. T. Linteris and D. Reinelt, Chemical limits to flame inhibition, **Combustion and Flames**, 115, (1998), pp. 551-560.

9. Marc D. Rumminger, and Gegory T. Linteris, The role of particles in the inhibition of counterflow diffusion flames by iron pentacarbonyl, **Combustion and Flames**, 128 (2002), pp.145-164.

10. Maria U. Alzueta, Rafael Bilbao, and Peter Glarborg, Inhibition and sensitization of fuel oxidation by SO_2, **Combustion and Flames**, 127 (2001), pp. 2234-2251.

11. G. O. Thomas, The quenching of laminar methane-air flames by water mists, **Combustion and Flames**, 130 (2002), pp. 147-160.

12. J. Andrae and P. Björnbom, Numerical studies of wall effects with laminar methane flames, **Combustion and Flames**, 128 (2002), pp. 165-180.

13. D. P. Mishra and A. Rahman, An experimental study of flammability limits of LPG/Air mixtures, **Fuel**, 82 (2003), pp. 863-866.

14. Ramanan Sankaran and Hong G. IM, Dynamic flammability limits of methane/air premixed flames with mixture composition fluctuations, **Proceedings of the Combustion Institute**, Volume 29, (2002), pp. 77-84.

15. G.T Linteris, M.D. Rumminger, and V. Babushok, Flame inhibition by Ferrocene, alone with CO_2 and CF_3H, **Halon Options Technical Working Conference**, 2-4 May 2000, pp. 129-139.

16. W. Juchmann, H. Latzel, D. I. Shin, G. Peiter, T. Dreier, H. R. Volpp, J. Wolfrum, R. P. Lindstedt, and K. M. Leung, Absolute Radical Concentration Measurements and Modeling, **The Combustion Institute**, (1998) pp. 469-476.

17. Christine M. Vagelopoulos and Fokion N. Egolfopfulos, Direct Experimental Determination of Laminar Flame Speeds, **The Combustion Institute**, (1998) pp. 513-519.

18. M. Fairweather, G. . Hargrave, S. S. Ibrahim, and D. G. Walker, Studies of Premixed Flame Propagation in Explosion Tubes, **Combustion and Flames**, 116: (1999) pp 504-518.

19. Y. N. Shebeko, S. G. Tsarichenko, A. Ya. Korolchenko, A. V. Trunev, V. Yu. Navzenya, S.N. Papkov, and A. A. Zaitzev, Burning velocities and flammabilitylimits of gaseous mixtures at elevated temperatures and pressures, **Combustion and Flames**, 102, (1995) pp. 427-437.

20. K. K. Kuo, **Principles of Combustion**, 1st ed. John Wiley & Sons, 1986.
21. A. Sakhrieh, Reduction of Pollutant Emissions from High Pressure Flames using an Electric Field, **PhD Thesis, Erlangen (2006), Germany**.

22. J. F. Griffiths and J. A. Barnard, **Flame and Combustion**, 3rd ed. Blackie Academic and Professional , an imprint if Chapman & Hall, 1995.

23. I. Glassman, **Combustion**, 2nd ed. Academic Press Inc., Florida, 1987.

24. F. A. Williams, **Combustion theory**, 2nd ed. Addison-Wesley Publishing Company, California, 1985.

25. A. M. Garforth, and C. J. Rallis, Laminar burning velocity of stoichiometric methane air: pressure and temperature dependence, **Combustion and Flames**, 31, (1978) pp. 53-68.

26. I. Toshio and T. Takeno, Effect of temperature and pressure on burning velocity, **Combustion and Flames**, 65, (1986) pp. 35-43.

27. D. K. Kuehl, Laminar burning velocities of propane air mixtures, **Proceeding of Combustion Institute**, 8, (1960) pp. 510-521.

28. G. E. Andrews and E. Bradley, The burning velocity of methane air mixtures, **Combustion and Flames**, 19, (1972) pp. 275-288.

29. P. Hill and J. Huang, **Combustion Science and Technology**, 60, (1980) pp. 7-30.

30. A.C. Egerton and D. Sen, Flame propagation: the influence of pressure on the burning velocity of flat flames, **Proceeding of Combustion Institute**, 4, (1952) 321-328.

31. M. Gilbert, The influence of pressure on flame speed, **Proceeding of Combustion Institute**, 6, (1957) 74-83.

32. F. N. Egolfopoulos, P. Cho, and C. K. Law, Laminar flame speeds of methane air mixtures under reduced and elevated pressure. **Combustion and Flames**, 76, (1989) 375-391.

33. G. L. Dugger, Effect of initial mixture temperature on flame speed of methane-air, propane-air, and ethylene-air mixtures, **National Advisory Committee for Aeronautics (NACA) Report**, 1061, (1950) pp. 105-116.

34. G. L. Dugger, Effect of initial mixture temperature on flame speed and flame blow-off limits of propane-air mixtures, **National Advisory Committee for Aeronautics (NACA) Technical note**, 2170 (1950).

35. M. Metghalchi and J. C. Keck, Laminar burning velocity of propane-air mixtures at high temperature and pressure. **Combustion and Flames**, 38, (1980) pp. 143-154.

36. G. P. Smith, D. M. Golden, M. Frenklach, N. W. Moriarty, B. Eiteneer, M. Goldenberg, C. T. Bowman, R. K. Hanson, S. Song, W. C. Jr. Gardiner, V. V. Lissianski and Z. Qin, GRI-Mech an optimized detailed chemical reaction mechanism for methane combustion. **Gas Research Institute** 1999, see also GRI Mech. Homepage **http://www.me.berkely.edu./gri_mech/releases.html**.

37. K. Seshadri and N. Peters, The inner structure of methane air flames, **Combustion and Flames**, 81 (1990) pp. 96-118.

38. N. Peters and F. A. Williams, The asymptotic structure of stoichiometric methane-air flames, **Combustion and Flames**, 68 (1987) pp. 185-207.

39. **http://en.wikipedia.org/wiki/Explosive_limit**

40. **http://www.engineeringtoolbox.com/explosive-concentration-limits-d_423.html. http://en.wikipedia.org/wiki/Flame_speed.**

41. Hamdan M. A. S. Inhibitory Effects of Inorganic Halogen Compound on H_2-Air and CH_4-Air Mixtures. **Master Thesis, (1977) University of Leads, UK.**

42. G. L. Borman, and K W. Ragland, **Combustion Engineering**, International ed. McGraw Hill Inc. (1998).

43. Dabbas R, Inhibition of gaseous combustion mixture using certain additives. **Master Thesis, (1999), University of Jordan, Jo.**

44. **http://en.wikipedia.org/wiki/Flame_retardant.**

44. Gregory Linteris, Marc Rumminger , Valeri Babushok , Harsha Chelliah, Tony Lazzarini, and Pasan Wanigarathne, Effective Non-Toxic Metallic Fire Suppressants, **Building and Fire Research Laboratory, Mechanical and Aerospace Engineer, (2002) University of Virginia, Virginia, US.**

45. Gregory T. Linteris, Vadim Knyazev, and Valeri Babushok 2001, Premixed flame inhibition by manganese and tin compounds, **National Institute of Standards and Technology.**

46. James W. Fleming, Mark D. Reed,' Eric J.P. Zegers,b Bradley A. Williams, and Ronald S. Sheinson. 1997 extinction studies of propane/air counterfzow diffusion flames: the effectiveness of aerosols, **Navy Technology Center for Safety and Survivability Combustion Dynamics Section, Washington, USA.**

47. Noto T, Babushok , Vurcess J , Iiamins A , and Tsang W.1985. Effect of halogenated flame inhibitors on organic flame, **National institute of standard and technology, Gaithersburg, USA.**

48. O. P. Korobeinichev, V. M. Shvartsberg, A.G. Shmakov, T.A. Bolshova.1995. Flame Inhibition by Phosphorus-Containing Compounds in Lean and Rich Propane Flames, **Institute of Chemical Kinetics & Combustion, Novosibirsk, Russia.**

APPENDICES

A.1 Chemical Kinetics Software

At its most fundamental level, CHEMKIN software enables the simulation of complex chemical reaction. With the advanced capabilities now available, sophisticated design-of-simulation (DoS) can be created to parametrically expore potential design solutions well before costly hardware is built.

CHEMKIN evolved from its origin as a Sandia National Laboratory combustion code (Chemkin II) into today's commercial-quality software suite with a yser friendly interface, best in class simulation speed, and unparalleled accuracy. No other chemistry solutions product is more widely validated or cited in technical peer-reviewed journals.

A.2 GRI-Mech.

GRI-Mech is an optimized detailed chemical reaction mechanism capable of the best representation of natural gas flames and ignition that are able to be provide at this time.

GRI-Mech is essentially a list of elementary chemical reactions and associated rate constant expressions. Most of the reactions listed have been studied one way or another in the laboratory, and so the rate constant parameters mostly have more or less direct measurements behind them.

GRI-Mech 3.0 is an optimized mechanism designed to model natural gas combustion, including NO formation and reburn chemistry.

It is the successor to version 2.11, and another step in the continuing updating evolution of the mechanism.

A.3 Some Fuels Flammability Limits

Fuel Gas	"Lower Explosive or Flammable Limit" (LEL/LFL) (%)	"Upper Explosive or Flammable Limit" (UEL/UFL) (%)
Isopropyl Alcohol	2	12
Gasoline	1.4	7.6
Kerosine	0.7	5
Methane	5	15
Methyl Alcohol	6.7	36
Methyl Chloride	10.7	17.4
Methyl Ethyl Ketone	1.8	10
Naphthalene	0.9	5.9
n-Heptane	1.0	6.0
n-Hexane	1.25	7.0
n-Pentene	1.65	7.7
Neopentane	1.38	7.22
Neohexane	1.19	7.58
n-Octane	0.95	3.20
iso-Octane	0.79	5.94
n-Pentane	1.4	7.8
iso-Pentane	1.32	9.16
Propane	2.1	10.1
Propylene	2.0	11.1
Silane	1.5	98
Styrene	1.1	6.1
Toluene	1.27	6.75
Triptane	1.08	6.69
p-Xylene	1.0	6.0
Fuel Oil No.1	0.7	5

A.4 Thermodynamic Data Files

Thermodynamic data file is a set all data that can be ever found for chemicals related to thermodynamic properties and quantities. It is a free of charge database contains ideal gas thermochemical database with updates from active thermochemical s.

Database used in the simulation is 'Alexander Burcat and Branko Ruscic' one. The latest print quotation to be made to this database is: Third Millennium Ideal Gas and Condensed Phase Thermochemical Database for Combustion with updates from Active Thermochemical s.

The used database started with the following definition:

"The latest print quotation to be made to this database is: Alexander Burcat and Branko Ruscic "Third Millennium Ideal Gas and Condensed Phase Thermochemical Database for Combustion with updates from Active Thermochemical s" ANL-05/20 and TAE 960 Technion-IIT, Aerospace Engineering, and Argonne National Laboratory, Chemistry Division, September 2005".

A.5 Transport Data Files

Transport data file is a set of species that has transport properties, these properties are of importance for simulation, and they are found in many forms and quantities. The used one here is Konnov Transport parameters, referred to Konnov from Belgium.

The used data base started with the following samples:

```
" AR              0   136.500     3.330     0.000     0.000     0.000
 OH               1    80.000     2.750     0.000     0.000     0.000
C                 0    71.400     3.298     0.000     0.000     0.000 ! *"
```

A.6 CO_2 Chemical Reactions

Chemical reactions of CO_2 taken into consideration was according to The CRC Handbook of Chemistry and Physics 89th edition (Internet Version 2009), CRC Press/Taylor and Francis, FL.:

CO_2 Reactions

$CO+O+M=CO_2+M$

$CO+O+AR=CO_2+AR$

$CO+O_2=CO_2+O$

$CO+OH=CO_2+H$

$CO+HO_2=CO_2+OH$

A.7 N_2 Chemical Reactions

Chemical reactions of N_2 taken into consideration was according to The CRC Handbook of Chemistry and Physics 89th edition (Internet Version 2009), CRC Press/Taylor and Francis, FL.:

N_2 Reactions

$NO+H=N+OH$

$NO+O=N+O_2$

$N+HO_2=NO+OH$

$NO+N=N_2+O$

$N_2+O=NO+N$

$N+O_2=NO+O$

$NO+NO=N_2+O_2$

A.8 SO_2 Chemical Reactions

Chemical reactions of SO_2 taken into consideration was according to The CRC Handbook of Chemistry and Physics 89th edition (Internet Version 2009), CRC Press/Taylor and Francis, FL.:

SO_2 Reactions

$SO+O+M=SO_2+M$

$SO+OH=SO_2+H$

$SO+O2=SO_2+O$

$SO_2+CO=SO+CO_2$

$SO+NO_2=SO_2+NO$

$SO+SO=SO_2+S$

A.9 Low Temperature (<1500K) Reaction Pathway Diagram for Combustion of CH_4

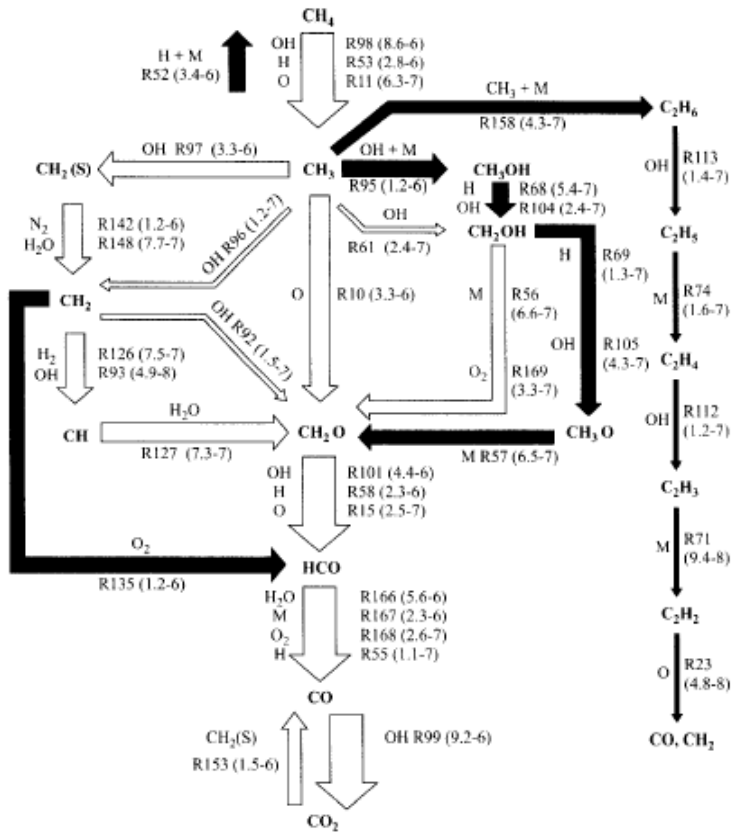

$$CH_4 \xrightarrow{OH,H,O} CH_3$$
$$CH_3 \xrightarrow{OH,M} CH_3OH$$
$$CH_3 \xrightarrow{OH} CH_2$$
$$CH_3 \xrightarrow{OH} CH_2O$$
$$CH_2 \xrightarrow{OH,H_2} CH$$
$$CH_2 \xrightarrow{O_2} HCO$$
$$CH \xrightarrow{H_2O} CH_2O$$
$$CH_3OH \xrightarrow{OH,H} CH_2OH$$
$$CH_2OH \xrightarrow{OH,H} CH_3O$$
$$CH_3O \xrightarrow{M} CH_2O$$
$$CH_2O \xrightarrow{OH,H,O} HCO$$
$$HCO \xrightarrow{H_2O,M,H,O_2} CO$$
$$CO \xrightarrow{OH} CO_2$$
$$CO \xrightarrow{OH} CO_2$$

The radicals depend on a simplified methane mechanism, and the selected referenced mechanism corresponds to maximum number of radicals that could affect the elementary methane reaction mechanism [3].

" تأثير إضافة بعض المواد على فاعلية إخماد لهب خليط غاز الميثان مع الهواء "

إعداد

إسماعيل إبراهيم حسن هديب

المشرف

الأستاذ الدكتور محمد أحمد حمدان

المشرف المشارك

الدكتور جهاد أحمد يامين

ملخص

تم إجراء دراسات تأثير الإخماد لبعض الغازات المحلية على تنامي شعلة خليط غاز الميثان والهواء في الأنبوب الرأسي نظرياً وعملياً . الغازات المخمدة المستخدمة في هذه الدراسة كانت غاز ثاني أكسيد الكربون وغاز النيتروجين وغاز ثاني أكسيد الكبريت . تم عمل هذه الدراسة بإيجاد حدود الاشتعال وسرعة الشعلة لكل من خليط غاز الميثان والهواء النقي ، وخليط الميثان والهواء والغاز المخمد ، تم تغيير تراكيز الغاز المخمد ما بين 5% إلى 20% من حيث الحجم .

تم بناء جهاز تجارب من الزجاج بالإضافة إلى تركيب أجهزة قياس في أماكن مختلفة ، والتي استخدمت لإيجاد سرعة الشعلة وحدود الاشتعال . أسطوانات الغاز المستخدمة كانت من الميثان بنسبة نقاء 99.94% وثاني أكسيد الكربون بنسبة نقاء 99.92% والنيتروجين بنسبة نقاء 99.93% . أولاً، تم تحديد أساس للمقارنة ، بدراسة احتراق خليط غاز الميثان والهواء النقي وسرعة شعلته وقياس حدود الاشتعال . ثم تم إضافة كمية من معروفة الغاز المخمد بدورها وتم قياس نفس البيانات . وقد تمت كل التجارب السابقة في ظروف الضغط الجوي .

وُجد أن سرعة شعلة خليط غاز الهواء والميثان النقي في التنامي الرأسي 0.4 م/ث. وقد قلت هذه القيمة بإضافة الغاز المخمد . وُجد أن الحد الأدنى للاشتعال هو 5% والحد الأعلى للاشتعال هو 14% لشعلة الميثان والهواء النقية عند تنامي الشعلة للأعلى . وعندما استخدم غاز ثاني أكسيد الكربون بالنسب (5 ، 10 ، 15 ، 20%) كانت الحدود الأدنى للاشتعال (5.4 ، 5.8 ، 6.1 ، 7.1%) على الترتيب ، وكانت الحدود الأعلى للاشتعال (13.2 ، 12.5 ، 11.6 ، 10.0%)

على الترتيب . وعند استخدام النيتروجين بنفس النسب المئوية ، كانت الحدود الأدنى للاشتعال (5.3 ، 5.6 ، 6.0 ، 6.7%) على الترتيب ، وكانت الحدود الأعلى للاشتعال (13.5 ، 13.0 ، 12.8 ، 12.0%) على الترتيب .

للحصول على نظرة داخلية لما يحدث داخل منطقة التفاعل ، تم استخدام النموذج النظري المكون من النسخة الأخيرة من GRIMech وهي ميكانيكية تفاعل احتراق الميثان . تم تهيئة وتعديل كل ملفات البيانات وتشمل الخواص الحرارية والخواص الانتقالية ، ومدخلات المكونات الكيميائية ، وشكل وأبعاد الأنبوب والشروط الابتدائية وميكانيكية التفاعل ، بالتناظر مع النتائج العملية . هذه الملفات (شاملة ميكانيكية التفاعلات) تم تعديلها عند استخدام كل غاز مخمد بدوره (ما عدا غاز SO_2) وتم التحقق منها بالتناظر مع النتائج التجريبية .

وُجد أن غاز CO_2 يملك أعلى تأثير إخماد وأن غاز N_2 له أقل تأثير إخماد بين المخمدات المستخدمة في هذا العمل . غاز SO_2 له تأثير إخماد جيد مقارنة بغاز النيتروجين لكنه يبقى ضعيفاً بالمقارنة مع غاز ثاني أكسيد الكربون . ويكون الترتيب الإخمادي للغازات المخمدة الثلاث المستخدمة هو $CO_2 > SO_2 > N_2$.